Biogeosciences Discuss., 10, 10531–10579, 2013
www.biogeosciences-discuss.net/10/10531/2013/
doi:10.5194/bgd-10-10531-2013

Biogeosciences Discussions
Open Access

Using a two-layered sphere model to investigate the impact of gas vacuoles on the inherent optical properties of *M. aeruginosa*

M. W. Matthews[1] **and S. Bernard**[1,2]

[1]Marine Remote Sensing Unit, Department of Oceanography, University of Cape Town, Rondebosch, Cape Town, 7701, South Africa
[2]Earth Systems Earth Observation, Council for Scientific and Industrial Research, 15 Lower Hope Street, Rosebank, 7700, Cape Town, South Africa

Received: 22 May 2013 – Accepted: 10 June 2013 – Published: 27 June 2013

Correspondence to: M. W. Matthews (mttmar017@myuct.ac.za)

Published by Copernicus Publications on behalf of the European Geosciences Union.

Abstract

A two-layered sphere model is used to investigate the impact of gas vacuoles on the inherent optical properties (IOPs) of the cyanophyte *Microcystis aeruginosa*. Enclosing a vacuole–like particle within a chromatoplasm shell layer significantly altered spectral scattering and increased backscattering. The two-layered sphere model reproduced features in the spectral attenuation and volume scattering function (VSF) that have previously been attributed to gas vacuoles. This suggests the model is good at least as a first approximation for investigating how gas vacuoles alter the IOPs. The central value of the real refractive index, $1 + \epsilon$, for the shell layer was determined using a radiative transfer model and measured remote sensing reflectance, R_{rs}, and IOP data. For a cell with 50 % vacuole volume, the mean $1 + \epsilon$ value for the shell layer was 1.12. The corresponding chl *a* specific phytoplankton backscattering coefficient, $b^*_{b\phi}$, ranged between 3.9×10^{-3} and 7.2×10^{-3} m^2 mg^{-1} at 510 nm. This agrees closely with in situ particulate backscattering measurements and values reported elsewhere. R_{rs} simulated for a population of vacuolate cells was greatly enlarged relative to a homogeneous population. Empirical algorithms based on R_{rs} were derived for estimating chl *a* in eutrophic/hypertrophic waters dominated by *M. aeruginosa*. The study confirms that gas vacuoles cause significant increase in backscattering and are responsible for the high R_{rs} values observed in buoyant cyanobacterial blooms. Gas vacuoles are therefore one of the most important bio-optical substructures influencing the IOPs in phytoplankton.

1 Gas vacuoles in cyanobacteria: implications for light scattering

Light scattering by planktonic algae and cyanobacteria is profoundly influenced by internal structure (Svensen et al., 2007; Whitmire et al., 2010). Intracellular gas vacuoles are know to have a pronounced effect on the interaction of light with cyanobacteria cells (Dubelaar et al., 1987; Ganf et al., 1989; Volten et al., 1998). Gas vacuoles in cyanobacteria are potentially one of the most important distinctive cellular structures

BGD
10, 10531–10579, 2013

influencing the inherent optical properties (IOPs), namely absorption (a), scattering (b), and backscattering (b_b). Absorption spectra collected using an integrating sphere (which collects all of the forward scattered light) showed reduced absorption following collapse of vacuoles in a wavelength–independent fashion (Dubelaar et al., 1987). This is attributed to the loss of light that is scattered in a backward direction by vacuoles which is confirmed by measurements of isolated collapsed gas vesicles which have insignificant absorption (Waaland et al., 1971; Shear and Walsby, 1975; Walsby, 1994). Therefore intracellular vacuoles probably only lead to a slight increase in true cellular absorption (Ogawa et al., 1979).

Vacuoles have a far greater effect on attenuation than on absorption as a result of strong spectral scattering (see figures in Waaland et al., 1971; Shear and Walsby, 1975; Ogawa et al., 1979; Dubelaar et al., 1987; Ganf et al., 1989; Walsby, 1994). Observations of natural turbid waters dominated by *Microcystis* spp. indicate that vacuoles may contribute up to 80 % of light scattering (Ganf et al., 1989). Gas vacuoles may scatter up to six times the light scattered by the cell (Fogg et al., 1973). Attenuation is generally increased by the presence of vacuoles (Waaland et al., 1971; Shear and Walsby, 1975; van Liere and Walsby, 1982; Walsby, 1994), however the results of Dubelaar et al. (1987) suggest the changes are more complex (initial decrease followed by an increase). The difference spectra between vacuolate and non-vacuolate suspensions (which can be attributed to scattering) are typically flat with troughs corresponding to the absorption maxima of cellular pigments (Walsby, 1994; Waaland et al., 1971; Shear and Walsby, 1975). The spectral shapes of the difference curves resemble inverted absorption curves and are similar to scattering spectra of algae (e.g. Bricaud et al., 1983; Zhou et al., 2012). Therefore it appears that vacuoles contained in the cell increase the overall scattering of the cell suspensions equally across the spectrum. This is in contrast to the scattering properties of isolated gas vesicles, which scatter light as Rayleigh scatterers with a λ^{-4} shape. When vesicles are packaged within the cell wall in honeycomb-like vacuole arrangements however, their scattering properties

BGD
10, 10531–10579, 2013

change. This is most likely caused by the increased particle size of vacuole arrangements (Shear and Walsby, 1975).

The effect of gas vacuoles on angular light scatter was examined using flow cytometry by Dubelaar et al. (1987); Dubelaar and van der Reijden (1995). Collapse of vacuoles in cultured *M. aeruginosa* suspensions increased forward light scatter by a factor of five while simultaneously decreasing perpendicular light scatter by a factor of ten. The reduced forward light scatter is attributed to a reduction in the real refractive index, n, of the cell as a whole as a result of the gas vacuoles. More detailed measurements of the volume scattering function (VSF) of vacuolate and non-vacuolate *M. aeruginosa* cells reveal significant changes in the shape of the VSF (Volten et al., 1998; Schreurs, 1996). Vacuolate cells consistently show a flattening of the VSF in the forward direction, which corresponds to the reduced forward light scatter measured by Dubelaar et al. (1987). This phenomenon is only reproduced by Mie modelling using homogeneous spheres with very low refractive index (= 0.4) relative to water (Schreurs, 1996). This confirms that the reduced forward light scatter is caused by vacuoles which reduce the overall real refractive index of the cell.

There is also evidence that the presence of vacuoles strongly enhances spectral backscattering of cyanobacteria. In comparison with other phytoplankton, vacuolate *M. aeruginosa* is among the most efficient scatterers and is the most efficient backscatterer (Zhou et al., 2012). Matthews et al. (2012) measured a mean chl *a* specific particulate backscatter (b^*_{bp}) in dense *M. aeruginosa* blooms of 0.4×10^{-3} m^{-1} at 420 nm and 1.98×10^{-3} m^{-1} at 700 nm (N = 13). These were an order or magnitude larger than similar measurements made in a high biomass dinoflagellate marine bloom and are in the upper range of values present in literature (e.g. Whitmire et al., 2010; Ahn et al., 1992). The enhanced backscatter can be partially attributed to the small cell size, but must be overwhelmingly attributed to intracellular vacuoles, since *M. aeruginosa* has no other unusual substructure or shape variation (spherical) to distinguish it from algae. Unfortunately Zhou et al. (2012) did not measure the backscatter of non-vacuolate cells. Until

BGD
10, 10531–10579, 2013

the present study, no detailed modeling study has been undertaken to demonstrate the effect vacuoles might have on the IOPs of cyanobacteria.

1.1 Composition, morphology and cellular arrangement of gas vacuoles

Gas vacuoles are composed of individual gas vesicles which are stacked length–wise in a hexagonal honeycomb–type arrangement within the cytoplasm (see review by Walsby, 1994). These vesicles are cylindrical membrane tubes composed entirely of proteins and capped on each end with a half-cone. In *Microcystis* individual vesicles have width and height of approx. 70 and 360 nm, respectively, while the membrane wall is approx. 2 nm thick (Jost and Jones, 1970). Waaland et al. (1971) found a peripheral cellular arrangement of vacuoles in *Nostoc* cells, as was observed in the marine cyanobacterium *Trichodesmium* (Van Baalen and Brown, 1969). The peripheral arrangement of vacuoles has caused speculation of light–shielding of the photosynthetic lamella (e.g. Van Baalen and Brown, 1969; Rajagopal et al., 2005) however this is somewhat disputed (Ogawa et al., 1979). Polar arrangement is observed in *Pseudanabaena* while both central and polar arrangements exist in *Oscillatoria* species (Meffert et al., 1981). In *M. aeruginosa* peripheral (Jost and Jones, 1970) and random (Jost and Zehnder, 1966; Šmarda, 2009) arrangements are observed. The main factor affecting the cellular arrangement of vacuoles appears to be the light conditions, with some evidence that high light favors a peripheral location (see Shear and Walsby, 1975; Walsby, 1994).

The ratio of gas vacuole to cell volume, $V_g : V_c$, also appears to be regulated by light as well as nutrient availability (Walsby, 1994). Density calculations for various cyanobacteria show that the volume occupied by vacuoles in order to make the cell neutrally buoyant varies from 3–10 % (ibid.). However, studies show that the actual volume occupied by vacuoles is often substantially higher than this. The volume occupied by vesicles in cultured *M. aeruginosa* in logarithmic growth phase was 5.8 μm^3 per cell which equates to $V_g : V_c$ = approx. 8 % (assuming a cell radius = 2.58 µm) (Lehmann and Jost, 1971). Gas vacuoles exist throughout the life cycle of *M. aeruginosa* in vari-

BGD
10, 10531–10579, 2013

able amounts reaching > 90 % of the cell volume in peak summer (Šmarda, 2009). Vacuoles are even present in the benthic overwintering stage in relatively high volumes ($V_g : V_c$ = 1.8–2.9 %) (Reynolds et al., 1981).

One of the primary consequences of vacuolation is lowering of cellular density (providing buoyancy) and therefore the overall real refractive index. The refractive index of the vacuole is close to 1.1 (relative to air) while that of the medium (water) and other cellular material is close to 1.372 (Fuhs, 1969). This change in refractive index has substantial implications for how light interacts with the cell (Shear and Walsby, 1975; Porter and Jost, 1976; Dubelaar et al., 1987). Using the concept of a significant refractive index and the Gladstone-Dale volume equivalence formulation, the overall or homogeneous refractive index, n_m, can be calculated from its parts according to $n_m = \sum_j n_j v_j$ where v is the relative volume and j is the number of components (Aas, 1996). Increasing the vacuole content leads to a concentration of cellular material as vacuoles occupy space within the cytoplasm (Raven, 1987). Calculating the homogeneous refractive index of the cell using the values of Fuhs (1969) for the gas vacuole and chromatoplasm and $V_g : V_c$ ranging from 2–90 % gives n_m varying over a considerable range between 1.367–1.127 (or 1.02–0.84 relative to water). This demonstrates the considerable effect gas vacuolation may have on n_m. A detailed calculation of m for the gas vacuole and chromatoplasm is performed in Sect. 2.1.

1.2 The two-layered sphere model approximation

Lorenz-Mie modeling using a population of homogeneous spheres has been used extensively to model phytoplankton IOPs (e.g. Stramski et al., 2001). However, this approach is often criticised as being overly–simplistic since phytoplankton differ considerably in shape and internal structure from homogeneous spheres. Recent comparisons between Mie modeling and experimental results demonstrate the limitations of this approach to sufficiently simulate phytoplankton IOPs (e.g. Zhou et al., 2012; Whitmire et al., 2010). An alternative approach is therefore required to account for variation in internal structure (and shape) of phytoplankton cells.

BGD
10, 10531–10579, 2013

Two-layered and three-layered sphere models which simulate internal structures of the cell wall, the cytoplasm, and or the chloroplast can more adequately simulate phytoplankton IOPs (e.g. Quinby-Hunt et al., 1989; Kitchen and Zaneveld, 1992; Bernard et al., 2009). In particular the Aden–Kerker 2 layered sphere is probably the simplest geometrical arrangement capable of reproducing experimental IOPs (Quirantes and Bernard, 2006). The suitability of such a two-layered Aden–Kerker model for investigating the optical consequences of gas vacuoles is evaluated here.

The cellular arrangement of cyanobacteria and *M. aeruginosa* in particular provides a unique opportunity for the two-layered model to investigate the influence of vacuole substructure. The traditional assignment of the two spherical layers of the model to chloroplast and cytoplasm respectively (e.g. Bernard et al., 2009) is less suitable to prokaryotic cyanobacteria. The thylakoids in cyanobacteria are not arranged in strict membrane bound chloroplasts but rather occur in the intracytoplasmic membrane towards the periphery of the cell (the so-called chromatoplasm). Given this cellular arrangement, the opportunity arises for the core layer to be assigned to a vacuole–like particle, while assigning the shell layer to that containing the photosynthetic thylakoids and the cytoplasm. This is based on the assumption that the vacuole can be adequately simulated as a single homogeneous particle of spherical shape. However, the shape and organisation of the vacuole might actually lend itself to such an approximation. In comparison with isolated vesicles, the vacuole is more irregular and in some cases spherical in shape owing to vesicle stacking; organised in the cell in one or more discrete packages; and much larger than the tiny individual vesicles (up to 3.5 µm in diameter by volume calculation) (see figures in Šmarda, 2009; Reynolds et al., 1981). Therefore vacuoles behave as larger optical units (Shear and Walsby, 1975) and might be sufficiently approximated by a spherical core layer.

1.3 *M. aeruginosa*: a representative prototype for modeling

M. aeruginosa is a ubiquitous cyanophyte responsible for much of the concern related to toxin-production from cyano–blooms in freshwaters. Worldwide it represents

BGD
10, 10531–10579, 2013

a prolific species of great relevance to environmental monitoring and remote sensing applications. Its morphological characteristics – spherical shape, relatively small size, high vacuole content – make it well suited to modeling studies based on spherical geometries and for testing theories related to how vacuoles might affect the IOPs. Previous IOP modeling studies of cyanophytes have mainly been restricted to small marine species (picoplankton) (e.g. *Synechococcus*), useful because they are assumed to generally obey the assumptions of Mie theory (e.g. Morel and Bricaud, 1986; Morel et al., 1993; Stramski et al., 2001). However, these are not representative of the genera. There therefore seems to be a paucity in detailed IOP studies of the cyanobacteria, especially for larger ubiquitous freshwater species e.g. *Microcystis* or *Dolichospermum*. The prolific occurrence of *M. aeruginosa* blooms in South African reservoirs make it a convenient species for studies using natural populations. It therefore represents a convenient prototype for optical modeling while simultaneously being of great relevance to environmental applications owing to its abundance.

The existence of *M. aeruginosa* in nature in colonial arrangements undoubtedly has significant implications for its IOPs, especially when considering absorption effects related to the package effect (Kirk, 1975; Agusti and Phlips, 1992). Microcystis cells form colonies with great variability in size and shape, and cell densities can be as high as 3–5 cells per 1000 μm^3 (Reynolds et al., 1981). Analysing colony size using flow cytometry, Dubelaar and van der Reijden (1995) found that colonies appear to behave as a collection of individual cells, rather than as larger discrete optical units (see Fig. 1 therein). While the geometries used in flow cytometry are appreciably different from nature, for the purposes of this study it is assumed that *M. aeruginosa* blooms can be modelled as a population of single cells.

The aim of this paper is to test the hypothesis that gas vacuoles significantly alter the IOPs of *M. aeruginosa* by causing large changes in scattering. The study begins by investigating the effects of containing a gas vacuole–like particle within a two-layered sphere on the optical efficiency factors, chl *a* specific IOPs, and VSF of *M. aeruginosa*. The relative influence of a gas vacuole on the IOPs and R_{rs} is then discussed. The

BGD
10, 10531–10579, 2013

two-layered sphere model is then tuned with experimental IOPs and R_{rs} data using a radiative transfer model. This enables plausible values for the shell layer $1+\epsilon$ and the corresponding chl *a* specific backscattering for *M. aeruginosa* to be established.

2 Methods

2.1 Complex refractive index of *M. aeruginosa*

The complex refractive index, m, of phytoplankton may be determined from spectral absorption and particle size distribution (PSD) measurements using an inverse ADA model (Bricaud and Morel, 1986; Ahn et al., 1992). This is based on the ADA assumption that the central value (denoted $1+\epsilon$) of n relative to the medium (water) is close to 1 (i.e. $1+\epsilon \approx 1.334$). This assumption is generally valid for phytoplankton (Aas, 1996). While heavily vacuolate cells violate this assumption, it should be valid for non-vacuolate cells. Since vacuoles have an insignificant effect on true cellular absorption used by the method, an initial value for the refractive index of a homogeneous *M. aeruginosa* cell consisting of chromatoplasm and centroplasm (minus effects of gas vacuoles) was determined using the method of Bricaud and Morel (1986) as modified by Bernard et al. (2001). The final choice of the $1+\epsilon$ value for a vacuolate cell however was determined using the R_{rs} data (see Sect. 2.4).

The chl *a* specific phytoplankton absorption coefficient (a^*_ϕ) was determined for spring blooms of *M. aeruginosa* in Hartbeespoort Lake sampled during October 2010 when the species made up more than 90 % of the population as percentage as determined by microscopy. Chl *a* was determined in triplicate spectrophotometrically by extraction in boiling ethanol (Sartory and Grobbelaar, 1984). The quantitative filterpad technique was used to determine the spectral absorption coefficients of particulate matter between 350 and 850 nm using a Shimadzu UV-2501 spectrometer fitted with an integrating sphere (Mitchell et al., 2003). The pigmented component was determined by sodium hypochloride bleaching. The Whatman GF/F filterpad was assumed

BGD
10, 10531–10579, 2013

to be completely diffuse ($\beta = 2$) (Roesler, 1998). The integrating sphere collects almost all of the forwards scattered light, however it does not account for the loss by backscatter which may be caused by vacuoles (Dubelaar et al., 1987). However, no attempt was made to correct the absorption measurements for backscatter by vacuoles but its effects are investigated (Sect. 3.1).

A log-normal distribution of cells with diameters ranging from 3.2 to 8 µm was used to estimate the PSD for *M. aeruginosa*. The size range is based in measurements of individual *M. aeruginosa* cells previously made in Hartbeespoort lake (Robarts et al., 1984). The distribution was expressed in terms of the effective variance (v_{eff}) and radius (r_{eff}) (Bernard et al., 2007) which were set to 0.02 and 2.58 µm respectively. The log-normal distribution is generally suitable for representing mono–specific phytoplankton blooms (Bricaud and Morel, 1986; Ahn et al., 1992). The size distribution was scaled to give 1 mg chl *a* for the population (or the chl *a* specific PSD) using an intracellular chlorophyll density (c_i). The c_i value has large implications for n', the absorption and scattering efficiencies (Q_{a}, Q_{b}) and the chl *a* specific volume coefficients (Morel and Bricaud, 1986). Therefore an appropriate value for c_i must be chosen with care. Values for c_i for *M. aeruginosa* previously measured are 2.1 kg m^{-3} (Zhou et al., 2012), 3.2 kg m^{-3} (Agusti and Phlips, 1992), and 4.5 kg m^{-3} (Reynolds et al., 1981). These were computed from cellular volumes and chl *a* concentrations presented in the references and fall within the upper range of accepted values for phytoplankton (e.g. Morel and Bricaud, 1986). Values for marine pico-cyanobacteria are typically less than this around 1.15–1.78 kg m^{-3} (ibid.). The lowest c_i value of 2.1 kg m^{-3} was selected after analysing results produced by the different values, as discussed in Sect. 3.4.

The experimental mean absorption efficiency factor, $\overline{Q_{\mathrm{a}}}$, for *M. aeruginosa* was then calculated between 360 and 850 nm using the estimated chl *a* specific PSD and a^*_ϕ (Morel and Bricaud, 1986). n' was then calculated by fitting the experimental $\overline{Q_{\mathrm{a}}}$ to that modelled using the ADA. Δn was determined as a Hilbert transform of n' according to the Kramers-Kronig theory of anomalous dispersion (Bernard et al., 2001). An initial value for $1 + \epsilon$ was then determined by convergence of the modelled efficiency factors

BGD
10, 10531–10579, 2013

for attenuation, Q_c, and for the non-absorption equivalent, Q_c^{NAE}. The $1+\epsilon$ value was selected at wavelength where n' was smallest. This technique was used given the absence of further scattering or attenuation data. The final shell layer $1+\epsilon$ value was determined as in Sect. 2.4.

2.2 Complex refractive indices of gas vacuoles

Using interference microscopy Fuhs (1969) estimated $n = 1.073$ for vacuole and $n = 1.372$ for the surrounding cytoplasm. Fuhs's (1969) calculations included the volumes of air, protein membrane and interstitial cytoplasmic material. The spectral refractive index for a hypothetical gas vacuole was calculated using a volume equivalent approach (Gladstone-Dale). Calculations were performed using the mean geometries for *Microcystis* vesicles given by Jost and Jones (1970) (length = 360 nm, diameter = 70 nm, wall thickness = 1.8 nm) and an assumed packing efficiency of 15 % (Walsby, 1994). Using these geometries, the relative volume for interstitial cytoplasm (water), air and proteins was calculated as 0.15, 0.76 and 0.09 respectively. The spectral real and imaginary refractive indices for the lipid-free protein Ovalbumin (Arakawa et al., 2001) were used for the protein membrane. These data are similar to values reported elsewhere for proteins ($n = 1.6$ and $k = 1e^{-5}$ Aas, 1996) and are generally representative of lipid-free proteins. Detailed spectral refractive index data for water and air were taken from Ciddor (1996) and Hale and Querry (1973), respectively.

2.3 Parameterisation of the two-layered sphere model

A two-layered sphere model using the Aden and Kerker (1951) formulation and the code of Toon and Ackerman (1981) were used to calculate the IOPs (after Bernard et al., 2009) in a Fortran/Matlab environment (The MathWorks™). Inputs to the model are the radius of the core and shell layers, m for the core and shell layers, the wave number (wavelength) and angular resolution (which is 0.1°). The output is the dimensionless angular intensity parameters (i_1 and i_2) and the efficiency factors for attenua-

BGD
10, 10531–10579, 2013

tion and scattering (Q_b) from which the phase function (β), the backscattering probability ($\tilde{b}_b$), and the absorption and backscattering efficiencies (Q_a, Q_{bb}) can be calculated (see Morel and Bricaud, 1986, for calculations). Using the PSD and m for shell and core layers, the bulk IOPs (a, b, and b_b) for the cell population were calculated at a 5 nm resolution.

The core and shell layers were assigned to the vacuole and chromatoplasm, respectively. By assigning the layer with the higher refractive index to be the outer layer, the effect of the cell wall membrane which is known to have a great impact on scattering (Quinby-Hunt et al., 1989; Svensen et al., 2007) is more adequately simulated. Furthermore, in cyanobacteria the photosynthetic thylakoids are most often arranged in concentric anastomosing shells parallel to the cell wall (Golecki and Drews, 1982), and this kind of arrangement with some additional irregularity is observed in *M. aeruginosa* (Šmarda, 2009). The sometimes peripheral arrangement of gas vacuoles are not without enclosure by the layered cell wall membrane, and a random arrangement within the centroplasm is more frequently observed in *M. aeruginosa*. This favors a core assignment for the vacuole which may even be surrounded by the photosynthetic lamella (Smith and Peat, 1967).

The effects of altering the relative volume occupied by the gas vacuole, V_g, on the IOPs is investigated. The relative volumes of the core, $V_c (= V_g)$, and shell, V_s, layers were adjusted according to $V_c = 1 - V_s$. The core radius, r_c, may be calculated using the shell radius, r_s, and V_c by $r_c = r_s V_c^{1/3}$. Considering relative gas vacuole volumes in the range 1–50 %, and a population of cells with diameters between 3.2–8.0 µm, the diameters of the spherical core vacuole would range between 0.68–6.34 µm. This represents a particle in the realm of Mie scattering, with a minimum diameter comparable to the wavelength of visible light (680 nm), and in the anomalous diffraction domain.

It has been shown that the cell volume remains unchanged when gas vesicles are collapsed by pressurisation (Porter and Jost, 1976; Dubelaar et al., 1987). The synthesis of vesicles within the cell therefore decreases the relative volume occupied by the chromatoplasm, leading to a concentration effect on the absorbing material, assum-

BGD
10, 10531–10579, 2013

ing that the amount of absorbing material in the cell (c_i) remains constant. This effect must be accounted for in calculations when altering the relative volumes of core and shell layers. The equation relevant to a two-layered geometry relating n' to c_i and the relative shell volume, V_s, is given by (Bernard et al., 2009):

$$n'_{\text{chrom}}(675) = \frac{675}{n_{\text{media}}} \frac{c_i a^*_{\text{sol}}(675)}{\pi 4 V_s} \quad (1)$$

where $n_{\text{media}} = 1.334$ and $a^*_{\text{sol}}(675)$ is the theoretical maximum absorption by unpackaged chl *a*.

This scales the imaginary refractive index (n') at 675 nm by the maximum theoretical absorption of unpackaged chl *a*, keeping the amount of absorbing material in the cell constant. The value for $a^*_{\text{sol}}(675)$ is given by Johnsen et al. (1994) as 0.027 $\text{mg}^{-1}\,\text{m}^{-2}$ which is applicable to cyanobacteria (Bidigare et al., 1989).

2.4 Tuning of the two-layered sphere using R_{rs}

There is likely to be some uncertainty in the value of $1+\epsilon$ derived for a homogeneous cell using absorption data and the method of Bernard et al. (2001) as described in Sect. 2.1. Therefore, there is a need for the $1+\epsilon$ value to be tuned, especially when considering that the chromatoplasm is modelled as a shell layer and not a homogeneous sphere. The Ecolight-S (V1.0) (E-S) radiative transfer model (©Sequoia Scientific) was used together with measured IOPs and R_{rs} to tune the two-layered sphere model for *M. aeruginosa*. The optimum shell layer $1+\epsilon$ value was determined through fitting the measured and modelled R_{rs} using a look-up-table of $b^*_{\text{b}\phi}$ and b^*_{ϕ} values produced by the two-layer model. The LUT was generated through varying the shell layer $1+\epsilon$ value between 1.04 and 1.15 at a 0.001 interval. The volume occupied by the gas vacuole was kept constant at $V_g = 50\,\%$. Fitting of the modelled and measured R_{rs} was performed using a Nelder-Mead simplex optimisation algorithm though selecting values for $b^*_{\text{b}\phi}$ and b^*_{ϕ} from the LUT.

BGD
10, 10531–10579, 2013

Measurements of the tripton (TR) absorption (a_{tr}) were performed by sodium hypochloride bleaching as described in Sect. 2.1. The concentration of tripton dry mass (TR) was determined from seston dry mass (EPA, 1983) and chl *a* using a conversion factor for chl *a* to dry mass for *M. aeruginosa* of 0.09 g mg^{-1} (Zhang et al., 2009; Reynolds, 2006). An exponential function was used to estimate the mass-specific tripton absorption as $a^*_{tr} = 0.037e^{-0.010(\lambda-442)}$. The values determined for $a^*_{tr}(442)$ = 0.037 m^2 g^{-1} and the exponential slope coefficient = 0.010 nm^{-1} are in close agreement with literature values (e.g. Zhang et al., 2009; Dekker et al., 2002). The corresponding tripton mass-specific (back)scattering coefficients, b^*_{tr}, b^*_{btr} were calculated using an inverse ADA model (see Bricaud and Morel, 1986, for calculations). The tripton mass-specific PSD was computed using a^*_{tr} determined as above and an estimate of n' of 0.01 exp(−0.007λ) (Stramski and Wozniak, 2005) (note that the original equation given in Stramski et al., 2001, is incorrect). The tripton particles were assumed to obey a Jungian distribution with slope $\gamma = -4$ and diameters between 1 and 100 µm in log-spaced bins. Mie calculations of homogeneous spheres were then used with the mass-specific tripton PSD and n' to compute values for b^*_{tr} and b^*_{btr}. The real component of the refractive index was set to $n = 1.05$, assuming a 90 % detrital component ($n = 1.04$) and a 10 % mineral component ($n = 1.18$) (Stramski et al., 2001). The fit between the measured a^*_{tr} and that modeled by Mie calculations was very close ($R^2 = 0.98$). Power-law functions were fitted to the inverse model output and used in further modelling: $b^*_{tr} = 0.648\lambda^{-0.753}$ and $b^*_{btr} = 9.925e^{-4}\lambda^{-0.0816}$.

Absorption by gelbstoff (a_g) was measured using matched 10 cm quartz cuvettes filled with GF/F filtered sample and reference room temperature Milli-Q water. a_g was fitted using an exponential function and was further modelled as $a_g = a_g(442)e^{-0.017(\lambda-442)}$ using the value measured at 442 nm. The total IOPs were calculated according to a four component model, using the chl *a* specific coefficients for phytoplankton, the mass-specific coefficients for TR, and the corresponding measured

BGD
10, 10531–10579, 2013

values of chl *a*, TR and $a_g(442)$ (data unpublished):

$$a = \text{chl } a \times a^*_{\phi} + \text{TR} \times a^*_{\text{tr}} + a_g + a_w$$

$$b = \text{chl } a \times b^*_{\phi} + \text{TR} \times b^*_{\text{tr}} + b_w$$

$$b_b = \text{chl } a \times b^*_{b\phi} + \text{TR} \times b^*_{\text{btr}} + b_{bw}$$

Data for water, *w*, was taken from Rottgers et al. (2011).

R_{rs} was measured using an ASD FieldSpec3 (ASD Inc.) using the measurement geometry of Mueller et al. (2003). Briefly, 10 radiance spectra were collected in sequence for Spectralon™, sky and water targets. Taking care to exclude contaminated or outlying spectra, the mean of the radiance spectra for each target was computed, from which an R_{rs} spectrum was calculated. This procedure was performed in triplicate at each site, with the final R_{rs} spectrum determined as the mean. Measurements were made under mostly clear sky conditions (cloud cover < 20 %).

E-S was called as a subroutine in python programming language (V. 2.7.1). The vertical profile used was constant with depth. Atmospheric parameters used for calculating the downwelling irradiance were recorded at each station including the date, latitude, longitude, GMT, wind speed, aerosol optical thickness (AOT, Solar Light Microtops II sun photometer) and cloud cover (%). Horizontal visibility used by E-S was estimated by vis = 3.9449/(AOT500 − 0.08498) (Retalis et al., 2010). The air mass type was set to continental. Default values were used for atmospheric pressure (= 29.92 inches mercury), relative humidity (= 80 %), water vapor (= 1.5) and ozone.

The values determined for $b^*_{b\phi}$ were compared to the depth-specific particulate backscattering coefficient, $b_{bp}(z)$, measured at 440 and 700 nm using a Hydroscat 2 m (Hobilabs Inc.). Depth profiles ranging from the surface to a depth of approx. 5 m were binned, median filtered to reduce noise, re-sampled and interpolated to 10 log-spaced depth bins between 0.8 m and the maximum depth using nearest neighbour interpolation. The chl *a* specific particulate backscattering coefficients, b^*_{bp}, were calculated

BGD
10, 10531–10579, 2013

using b_{bp} at 0.8 m and chl *a* measurements made at the surface. Profiles measured with chl *a* in excess of 1500 mg m^{-3} were excluded from these calculations.

3 Results and discussion

3.1 Complex refractive indices

Figure 1 shows the data and results of the determination of the complex refractive indices for *M. aeruginosa* and the gas vacuole. The a^*_ϕ value (Fig. 1a) is well within the range presented in the literature for cyanobacteria (e.g. Dupouy et al., 2008), and is almost identical to that for *M. aeruginosa* determined by (Zhang et al., 2012), and slightly higher than values obtained by Dekker (1993) for eutrophic blue-green dominant assemblages. The characteristic absorption maximum of phycocyanin is clearly visible near 620 nm. The a^*_ϕ values used to calculate *m* did not account for increased apparent absorption that could result from backscatter by gas vacuoles. No attempt was made to correct the measurements for this effect. However, tests showed that variable a^*_ϕ has little effect on the value of $1 + \epsilon$ determined by the method. The significance of the variability in n' on the IOPs will be investigated further (Sect. 3.4).

The log-normal normalised PSDs are shown in Fig. 1b. The effects of varying V_{eff} is evident on the distribution shapes (r_{eff} is fixed at 2.58 µm). The narrow distributions are likely to be representative of the spring blooms in Hartbeespoort, and closely resemble those for monospecific cultures (e.g. Bricaud and Morel, 1986; Ahn et al., 1992). The value chosen for V_{eff} had a small influence on the values determined for Q_a and n' but caused more significant changes in $1 + \epsilon$ (between 1.078 and 1.081 for V_{eff} = 0.05 and 0.01 respectively). The value for V_{eff} was set to 0.02 so as to give a spread of smaller and larger cells without incurring a bias towards small cells, as is visible for V_{eff} = 0.05.

The experimental Q_a is shown in Fig. 1c, and agrees well with literature derived values for phytoplankton (ibid.). The imaginary refractive index (Fig. 1d) also compares well to the literature values for homogeneous and heterogeneous cells (Ahn et al.,

BGD
10, 10531–10579, 2013

1992; Bricaud and Morel, 1986; Bernard et al., 2009) and has a mean spectral value of $0.0012i$. The imaginary and real parts of the refractive index for the vacuole (Fig. 1d, e) have mean spectral values of $2.079e^{-5}i$ and 0.825 respectively. The value determined for the real part in air is 1.10, identical to that estimated by Fuhs (1969) to have the highest probability. These were estimated by power law functions in further modeling of the IOPs: $n' = 2.28e7\lambda^{-4.66} + 1.08e^{-5}$ and $n = 333\lambda^{-1.94} + 0.82$.

The value of $1+\epsilon$ for *M. aeruginosa* was determined as 1.080 (Fig. 1f). This value was determined at a wavelength of 625 nm where $n' = 0.001$. This value represents the mean homogeneous real refractive index of a *Microcystis* cell which includes the cell wall, thylokoids, the cytoplasm and other refractive cytoplasmic inclusions such as polyphosphate granules. The value is within the range of those presented elsewhere for algal cells (Morel and Bricaud, 1986; Bricaud et al., 1988), however it seems quite high when compared with values used previously for modeling cyanobacteria or *M. aeruginosa* as a homogeneous cell (e.g. Volten et al., 1998; Zhou et al., 2012). However, the value of 1.04 used by Volten et al. (1998) is an estimate for generic phytoplankton from Morel and Bricaud (1986). A value of 1.036 was determined by Zhou et al. (2012) for cultured *M. aeruginosa* using similar methods to those presented here, however none of the absorption, size or attenuation data used to constrain the final choice of $1+\epsilon$ was shown. More comparative values for $1+\epsilon$ between 1.047–1.085 are given by natural populations of marine *Chlorella* (Spinrad and Brown, 1986) which have similar shape (spherical) and size (d = 1.2–6.8 µm) to *M. aeruginosa*. A complex refractive index of $m = 1.085 + 0.048i$ was derived for a homogenous cell of marine *Chlorella* (Quinby-Hunt et al., 1989). Therefore $m = 1.080 - 0.0012i$ for a homogeneous *M. aeruginosa* cell between 400 and 750 nm is not outside the range of values determined for algae. The final value for $1+\epsilon$ for the shell layer of a vacuolate cell is determined using R_{rs} data (see Sect. 2.4).

BGD
10, 10531–10579, 2013

3.2 The influence of gas vacuolation on efficiency factors and volume coefficients

The optical efficiency factors versus the Mie size parameter ($\alpha = \pi d n_w/\lambda$, $n_w = 1.334$) for a single cell having variable gas vacuole content is shown in Fig. 2. The relative volume occupied by the gas vacuole is 0 %, corresponding to an essentially non-vacuolate homogeneous cell, 3 % for an upwardly buoyant cell, 10 and 30 % for an expected vacuole content in a buoyant surface bloom, and 50 % for a heavily vacuolate over-buoyant cell. The non-vacuolate cell ($V_g = 0$) demonstrates the expected interference patterns for Q_c and Q_b, tending towards theoretical expectations with increasing size. For cells with increasing vacuole content, there is significant perturbation in the phase, magnitude and shape of the efficiency factors. This is related to the internal gas vacuole, since the overall pigment content of the cell is constant. For a mean cell in the size range of *M. aeruginosa* Q_c and Q_b are slightly increased with increasing vacuolation, up to a point where they decreases dramatically with heavy vacuolation ($V_g = 50$ %). This is better observed by the spectral efficiency factors for the *M. aeruginosa* population shown in Fig. 3. The upward sloping Q_c and Q_b spectra are probably caused by the relatively high $1 + \epsilon$ value (Fig. 3a, b). This value has the greatest influence on the slope and shape of Q_c and Q_b (see Bricaud and Morel, 1986), and its influence is investigated further in Sect. 3.4. The value of $Q_c(510)$ ranges from 2.0–2.6 while that of $Q_b(510)$ ranges from 1.85–2.45 (table 1). Therefore according to the two-layered model, gas vacuoles can significantly alter the shape and magnitude of Q_c and Q_b through a shift in phase of the interference patterns of the efficiency factors (Fig. 2a, b). This finding is in agreement with Dubelaar et al. (1987) who found that gas vacuoles caused decreased overall spectral attenuation (see further analysis in Sect. 3.4). The shift in the position of the red chl *a* absorption induced attenuation feature near 685 nm towards shorter wavelengths is also visible with increasing vacuolation (Fig. 3a), as observed by Dubelaar et al. (1987). This confirms that gas vacuoles are responsible for this phenomenon.

BGD
10, 10531–10579, 2013

In accordance with theoretical expectations, Q_a is rather undisturbed by gas vacuolation, except for a very slight decrease with large heavily vacuolate cells (Figs. 2 and 3c). The agreement between the experimental and modelled Q_a is very close using a value of 0.022 for $a^*_{sol}(675)$. However, for gas vacuolation > 50 % there is a small departure from experimental values of Q_a (not shown). This effect is probably caused by a breakdown of the assumption of volume-equivalence (Eq. 1) rather than from light shielding or other effects. Therefore a maximum gas vacuole volume of 50 % was used for modeling, in order to not violate the volume equivalence assumption. It is apparent that gas vacuolation has very little implication for absorption according to the two-layered model, and therefore the model does not support a significant light shielding role for gas vacuoles in agreement with Ogawa et al. (1979).

The greatest effect of the gas vacuole is on Q_{bb} and the backward and forward scattering probabilities (Figs. 2, 3 d, e, f). $Q_{bb}(510)$ for a non-vacuolate cell ($= 7.3 \times 10^{-3}$) falls in the range of algal species modelled with relatively high refractive indices (see Ahn et al., 1992; Bricaud et al., 1988). Vacuolation increases Q_{bb} markedly in a relatively spectrally invariant and linear fashion and especially for smaller cell sizes in the range of *M. aeruginosa* (table 1). $Q_{bb}(510)$ for a heavily vacuolate cell (=0.0156) is twice that of its homogeneous equivalent. $\widetilde{b}_b$ may be up to 5 times larger in a heavily vacuolate cell than for a homogeneous equivalent in the size range of *M. aeruginosa* (Fig. 2e). This effect is associated with decreased $\widetilde{b_f}$ by up to 0.5 % (Fig. 2f), as was observed experimentally by Dubelaar et al. (1987). However, the spectral slope of $\widetilde{b}_b$ indicates enhanced backscattering with higher vacuole content towards the red relative to the blue (Fig. 3e). These curves closely resemble those determined experimentally (e.g. Zhou et al., 2012). The opposite is observed for forward scattering probability (Fig. 3f). Therefore the following can be said in relation to the effect of gas vacuoles on backscattering: firstly it appears that gas vacuolation has large implications for small cells of which *M. aeruginosa* is an example; secondly, Q_{bb} increases roughly linearly with increasing vacuole content; and lastly, $\widetilde{b}_b$ seems to be enhanced in the red relative to the blue for cells with a high gas vacuole content.

BGD
10, 10531–10579, 2013

The chl *a* specific volume coefficients for variable gas vacuolation are shown in Fig. 4a–d. The shapes of the attenuation and scattering spectra are identical to the efficiency factors in Fig. 3. The range of values for $b^*_{\phi}(510)$ from 0.25–0.33 $m^2\,mg^{-1}$ are towards the upper range of values observed for cyanophyta and phytoplankton in modelling studies (Morel and Bricaud, 1986; Bricaud et al., 1988). The downward–sloping attenuation curves for $V_g = 50\,\%$ resemble those previously measured for *M. aeruginosa* (Dubelaar et al., 1987). The modelled chl *a* specific absorption is almost identical to the measured value (see Fig. 1). $b^*_{b\phi}(510)$ is $1.0\times10^{-3}\,m^2\,mg^{-1}$ for a non-vacuolate cell, and $2.1\times10^{-3}\,m^2\,mg^{-1}$ for a heavily vacuolate cell. This amounts to a two–fold increase in $b^*_{b\phi}$ due to the presence of the gas vacuole. The values are within experimental values for phytoplankton (e.g. Whitmire et al., 2010) but are lower than those observed for *M. aerusinosa* by Zhou et al. (2012) ($= 5.727 \times 10^{-3}\,m^2\,mg^{-1}$) and the vacuolate marine cyanophyte *Trichodesmium* ($= 11 \times 10^{-3}\,m^2\,mg^{-1}$) (Dupouy et al., 2008). $b^*_{b\phi}$ is slightly negatively sloped but becomes more positively sloped towards the red > 700 nm with increasing vacuolation. Previous measurements of $b^*_{b\phi}$ for *M. aeruginosa* show a downward sloping spectral shape (Zhou et al., 2012). The change in n' and n due to vacuolation for the shell chromatoplasm layer is shown in Fig. 4e and f. The space occupied by the gas vacuole causes the absorbing material to be concentrated thereby increasing the value of n' which leads to associated changes in Δn. This assumes that the size of the cell remains unchanged by vesicle synthesis.

3.3 The influence of gas vacuolation on the VSF

There have been limited attempts to measure and model the scattering phase function (light scattering matrix) of *M. aeruginosa* both with and without gas vacuoles. Schreurs (1996) performed measurements presented in Volten et al. (1998) at 633 nm using an Helium-Neon laser to measure the VSF of vacuolate and pressurised (non-vacuolate) *M. aeruginosa* and another vacuolate *Microcystis* species. The presence of gas vacuoles was observed to cause unusual features in the VSF, specifically, an increase in

BGD
10, 10531–10579, 2013

magnitude between 20–70°, and a decline towards the forward direction < 40°. Similar to other studies citing the importance of intracellular structure on the scattering matrix (e.g. Quinby-Hunt et al., 1989; Witkowski et al., 1998; Svensen et al., 2007), these features have been speculatively attributed to gas vacuoles. The same studies used a population of homogeneous spheres using Lorenz-Mie theory to attempt to fit the measurements ($n = 1.04$, $n' = 0.000$). However, the homogeneous sphere model produced poor comparisons with measurements of both vacuolate and non-vacuolate cells. The flattening towards forward angle was only reproduced with a cell of significantly reduced real part of the refractive index (= 0.4) (Schreurs, 1996). The influence that gas vacuoles might have on the VSF in the extreme forward and backward directions remains unknown for the present. Although recently developed instruments have the capability to measure the VSF between 0.6–177° (e.g. Zhang et al., 2002), no such measurements on vacuolate and non-vacuolate cells appear to have yet been made.

Figure 5a–d shows the VSFs at four wavelengths. Three features attributable to the gas vacuole are immediately apparent: an enlargement between 20–70°, a flattening towards the forward direction < 45°, and a steady enhancement and flattening of the VSF in the backward direction > 90° for increasing vacuole content. The results are compared to those of Volten et al. (1998) in Fig. 5e, and normalised to the San Diego Harbour VSF at 90° (Petzold, 1972). The two-layer model for a vacuolate cell containing $V_g = 10\,\%$ accurately reproduces the enhanced scattering between 20–70°, as well as the flattening in the forward direction < 45° observed for vacuolate cells. The fit between the modelled homogeneous cell and the measured non-vacuolate cell is also good in the forward direction (< 90°). The enhancement in the backward direction from vacuoles is not observable in the measurements of Volten et al. (1998), and the magnitude of the measured VSF in the backward direction is substantially greater than that from the model. Tests varying some of the model's parameters and using those presented in Volten et al. (1998) (n=1.04, $n' = 0.000$, $V_{eff} = 0.92$, $R_{eff} = 6.83$) did not produce an improved fit. Nevertheless, the two-layered vacuole model accurately reproduces observations of the normalised VSF in the forward direction.

BGD
10, 10531–10579, 2013

3.4 Influence of the choice of $1+\epsilon$ and c_i on the IOPs

The value for $1+\epsilon = 1.036$ chosen by Zhou et al. (2012) was also used to calculate the IOPs for comparison with Sect. 3.1 (Fig. 6, Table 1). The resulting attenuation spectra compare more closely with the findings of Dubelaar et al. (1987) (Fig. 6a): the curves slope downwards towards the red; lower vacuole content results in gradually increased attenuation; and the shift of the attenuation peak caused by the absorption maximum of chl *a* towards shorter wavelengths with increasing vacuolation is clearly observed (681 nm for $V_g = 50\,\%$, 685 nm for $V_g = 0\,\%$). Therefore, gas vacuolation is likely the cause of these changes in attenuation. Spectral scattering is also decreased with increasing vacuolation in a manner similar to attenuation (absorption was constant) (Fig. 6b). The lower $1+\epsilon$ value results in substantially lower backscattering relative to the higher refractive index value (Fig. 6c, d). The heavily vacuolate cell ($V_g = 50\,\%$) scatters approximately the same as a non-vacuolate cell with the higher refractive index. The lower refractive index cell responds in much the same way as the cell with the higher refractive index to vacuolation with backscatter increasing in a roughly linear manner for increasing percentage vacuolation. The probability of backscatter for the lower refractive index cell is however more sloped, indicating a bias for light scatter in the red rather than in the blue. The VSF for the lower refractive index cell is generally smaller than for the higher refractive index cell, but less sloped in the backward direction (Fig. 6 e, f). The comparison with Volten et al.'s (1998) measured scattering function is poorer in the forward direction ($< \pi/2$) but slightly improved in the backward direction ($> \pi/2$). The distinctive features causing an enhancement and flattening in the VSF at forward angles is reproduced by the model.

The lower and higher refractive index cells respond in very similar ways to increasing gas vacuolation, and reproduce experimental observations in c and b, and in the VSF. The $1+\epsilon$ value controls both the shape of c and b, and the magnitude of b_b; therefore it is one of the primary causal variables, along with the vacuole itself, influencing the IOPs. Although the shape of spectral attenuation may be used to constrain the choice

BGD
10, 10531–10579, 2013

of $1+\epsilon$ (Bricaud and Morel, 1986) favouring a lower $1+\epsilon$ value, the higher $1+\epsilon$ value agrees better with measurements of the VSF and IOPs (Table 2). The final value for $1+\epsilon$ however is determined in Sect. 3.5 below.

The influence of c_i on the IOPs was also investigated using the values from Zhou et al. (2012) = 2.1 kg m^{-3}, Agusti and Phlips (1992) = 3.2 kg m^{-3} and Reynolds et al. (1981) = 4.5 kg m^{-3} (Table 2). The c_i value is directly linked to Q_a and causes changes in the values of n' and n due to the method used to determine m (Sect. 2.1). Higher c_i values give higher values for Q_a and therefore n', however the value determined for n is relatively unchanged (Table 2). The variable Q_a and n' values result in changes in the (back)scattering efficiencies and in the chl *a* specific IOPs produced by the two-layer model: higher c_i values are associated with lower Q_b and Q_{bb} values, and much smaller values for b^*_{ϕ} and $b^*_{b\phi}$ (Table 2). The changes in the chl *a* specific IOPs are primarily caused by normalising the PSD by chlorophyll. Therefore c_i has a large controlling influence on the two-layered model. The choice of c_i in this case was determined by the closeness to literature values of Zhou et al. (2012): the lowest c_i value = 2.1 kg m^{-3} most closely reproduced Zhou et al.'s (2012) Q_b = 2.26 and Q_{bb} = 0.02 values. A second reason for choosing the low c_i value is that higher c_i values were unable to reproduce the high values for $b^*_{b\phi}$ observed in buoyant *M. aeruginosa* blooms. The higher c_i values had a dampening effect on scattering probably due to the concentration of absorbing material in the shell layer. For these reasons the lower c_i value was used.

3.5 Determination of $1+\epsilon$ using R_{rs}

The value of $1+\epsilon$ of 1.08 determined for a homogeneous *M. aeruginosa* cell using the method of Bernard et al. (2001) gave $b^*_{b\phi}$ values lower than those observed experimentally. Initial simulations also showed the inability of the low $b^*_{b\phi}$ values to reproduce the high R_{rs} values measured in natural *M. aeruginosa* blooms. Therefore the value of $1+\epsilon$ for the shell layer of a vacuolate *M. aeruginosa* cell was tuned using measured R_{rs} and E-S simulations. The results of the modelled and measured R_{rs} are shown in

BGD
10, 10531–10579, 2013

Fig. 7a, b. In general, the spectral shapes of the modelled R_{rs} are in good agreement with measured R_{rs}. The difference between 400 and 750 nm is on average better than 0.005 sr^{-1}, which is likely to be satisfactory given the high R_{rs} values (Fig. 7c). There is no apparent consistent bias with wavelength; there is a good spread of over and under-estimates (Fig. 7d). The wavelength-specific coefficient of determination (Fig. 7e) has troughs in the regions corresponding to the fluorescence bands of phycobilipigments (550–650 nm) and chl *a* (near 685 nm). This is expected since the model does not account for fluorescence effects. The poor performance < 500 and > 700 nm is most likely related to strong combined gelbstoff and tripton absorption, and large uncertainties in $b^*_{b\phi}$ towards the NIR, respectively. It may also be related to the small sample size ($n = 8$). However, the correlation is sufficiently good between 500 and 700 nm to draw some conclusions related to the values of $1+\epsilon$ and the corresponding $b^*_{b\phi}$, especially since errors in the R_{rs} measurements themselves may be > 10 % depending on the wavelength and measurement conditions (Doxaran et al., 2004).

The mean value of $1+\epsilon$ determined using R_{rs} for the shell layer is 1.12 with a range between 1.104 and 1.138. The $1+\epsilon$ value is high when compared to typical values for homogeneous cells ($n = 1.06 \pm 0.04$) (Aas, 1996). Whether such a value is realistic must be considered in relation to the contributions made by the hard cell wall, the concentration effect of the gas vacuole on the chromatoplasm, and reported two-layer simulations. The typical value of n for a cell wall composed of protein is 1.2, which is the value used by Svensen et al. (2007) for the cell wall of a two-layer sphere. A shell layer with $n = 1.13$ and a core layer of $n = 1.08$ best reproduced the scattering matrix of *Chlorella*, a species with similar morphology to *M. aeruginosa* (Quinby-Hunt et al., 1989). Therefore, a value of 1.12 for the shell layer might be reasonable considering reported values of two-layer simulations. Such a high value is only feasible because of the presence of the gas vacuole, as the homogeneous value of n for the whole cell is less than one (0.97).

The corresponding $b^*_{b\phi}$ values are shown in Fig. 7f in comparison to the measurements of Zhou et al. (2012). The mean value of $b^*_{b\phi}(510)$ is 5.48×10^{-3} $m^2\,mg^{-1}$ with

BGD
10, 10531–10579, 2013

a range of 3.89×10^{-3} to 7.19×10^{-3} m^2 mg^{-1}. This is very close to that measured in cultures by Zhou et al. (2012) of 5.7×10^{-3} m^2 mg^{-1}. It is also within the range of values measured for *Microcystis* dominated assemblages in Spanish lake Rosarito (= 3.6 to 5.3 $\times 10^{-3}$ m^2 mg^{-1} at 412 nm) (personal communication Antonio Ruiz-Verdu). The estimated $b^*_{b\phi}$ values are also consistent with b_{bp} measurements (Fig. 8a, b). At 0.8 m $b^*_{bp}(440)$ ranged from 3.7×10^{-4} to 1.5×10^{-3} m^2 mg^{-1}, and $b^*_{bp}(700)$ from 1.9×10^{-3} to 7.8×10^{-3} m^2 mg^{-1}. These values are likely underestimates since chl *a* was measured at the surface, and the blooms were floating. Interestingly, b_{bp} is positively sloped towards the red near the surface and negatively sloped at depth (Fig. 8b). The explanation for this effect is not known, but seems to be related to biomass; if biomass affects the spectral slope then this finding has has important implications for measuring b_{bp} in cultures (Zhou et al.'s (2012) measurements were at chl *a* approx. 5 mg m^{-3}). In summary, the $b^*_{b\phi}$ values are typically larger or in the upper range of those determined experimentally for cultured algae (e.g. Whitmire et al., 2010; Vaillancourt, 2004), and are in good agreement with the limited measurements made on vacuolate *M. aeruginosa*.

Comparable values are found for $Q_b(510)$ and $Q_{bb}(510)$ determined using a two-layered sphere with shell layer $1 + \epsilon$ of 1.12 and those measured by Zhou et al. (2012) (Table 3). Zhou et al.'s (2012) b^*_{ϕ} values are substantially higher resulting in a smaller backscattering probability. It appears that the two-layered model has a lower total scattering due to the lower value of Q_b. The Q_{bb} value is in the upper range of those measured on algae cultures: from 0.0018–0.064 at 510 nm (Zhou et al., 2012; Vaillancourt, 2004) and from 0.006–0.061 at 442 nm (Whitmire et al., 2010). Surprisingly, the largest of these values are obtained from large dinoflagellates containing high intracellular carbon concentrations and unusual chromosome morphology and internal structures. Using similar reasoning, gas vacuoles are the explanation for the high backscatter efficiency of *M. aeruginosa*.

BGD
10, 10531–10579, 2013

4 Applications

4.1 Influence of gas vacuoles on reflectance

The large magnitude of R_{rs} and scattering in buoyant surface cyanobacterial blooms has been tentatively attributed to the presence of gas vacuoles (e.g. Ganf et al., 1989). The potential effect that intracellular gas vacuoles might have on the magnitude of R_{rs} was investigated through simulations for populations of vacuolate cells ($1+\epsilon$ of 1.12 and V_g = 50 %) versus non-vacuolate cells (homogeneous spheres, $1+\epsilon$ of 1.08). In the simulations, $a_{tr}(440)$ and $a_g(440)$ were set to constant values typical of Hartbeespoort of 0.5 and 1.5 m^{-1}, respectively. E-S was run using a solar zenith angle of 30°, a wind speed of 2 $m\,s^{-1}$, and default atmospheric parameters.

R_{rs} for vacuolate and non-vacuolate *M. aeruginosa* populations was computed for chl *a* between 20 and 1000 $mg\,m^{-3}$, a plausible range typically encountered in Hartbeespoort (Fig. 9a, b). The magnitude of R_{rs} for the vacuolate population is in the range observed in buoyant surface cyanobacterial blooms (see Wang et al., 2010; Matthews et al., 2010; Randolph et al., 2008; Zimba and Gitelson, 2006). A large difference in the magnitude of R_{rs} between the vacuolate and non-vacuolate populations is apparent, which becomes increasingly pronounced as the concentration of chl *a* increases. This effect is due solely to the increase in $b^*_{b\phi}$ associated with vacuolate cells. The peak near 710 nm becomes apparent around chl *a* = 30 $mg\,m^{-3}$ (note the model does not include fluorescence effects at 685 nm). For chl *a* > 500 $mg\,m^{-3}$, R_{rs} is enlarged significantly towards the NIR (> 700 nm). This is typical of surface *M. aeruginosa* blooms allowing them to be distinguished from other species of algae, e.g. dinoflagellates (Matthews et al., 2012). Therefore algorithms for detection/discrimination of vacuolate cyanophyte blooms might be targeted at the enlarged signal at these wavelengths (e.g. Matthews et al., 2012). The results demonstrate the large influence variable phytoplankton backscatter resulting from gas vacuoles may have on the magnitude of R_{rs}

BGD
10, 10531–10579, 2013

and provide an explanation for the high values observed in hypertrophic cyanobacteria-dominant waters.

4.2 Empirical algorithms for *M. aeruginosa*

While semi-analytical algorithms based on bio-optical models and solved using a variety of optimisation procedures are often used for deriving water constituents, forward modelled R_{rs} from bio-optical models also allow empirically based relationships to be established for water constituents (e.g. Matthews, 2011; Dekker et al., 2001). Empirical relationships between chl *a* and the 710 : 665 nm band ratio and the maximum peak height (MPH) variable drawn with baseline between 665 and 885 nm (Matthews et al., 2012), were derived from R_{rs} simulations for a population of vacuolate *M. aeruginosa*. E-S simulations were run for chl *a* between 20 and 1000 mg m^{-3} for vacuolate cells (see Sect. 4.1). $b^*_{b\phi}$ was extended to 900 nm in order to facilitate computation of the MPH variable using the value at 750 nm. $a_{tr}(440)$ and $a_g(440)$ were varied randomly in the ranges 0 to 2 m^{-1} and 0 to 5 m^{-1}, respectively, in order to simulate the natural variability that is expected for Hartbeespoort (Matthews, unpublished data), and to test the sensitivity of the empirical relationships.

Figure 10 shows the R_{rs} spectra and the empirical algorithms derived for the 710 : 665 ratio and the MPH variables. An exponential relationship was determined as the best fit for the 710 : 665 ratio:

$$\text{chl } a = 7.294 \times \exp^{1.2739 \times (R_{rs}(710)/R_{rs}(665))}, \quad R^2 = 0.99$$

A 2nd order polynomial (porabola) gave the best fit for the MPH variable:

$$\text{chl } a = 222\,173\,\text{mph}^2 + 5231.9\,\text{mph} + 14.625, \quad R^2 = 0.99$$

This relationship is similar to that derived using top-of-atmosphere MERIS data for *M. aeruginosa* dominant waters in Matthews et al. (2012). The empirical relationships are

BGD
10, 10531–10579, 2013

robust when subjected to random variation in tripton concentration and gelbstoff absorption. This is a result of the overwhelming contribution of cyanobacterial biomass to the IOPs as typically occurs in Hartbeespoort. The algorithms based on R_{rs} are likely to be applicable in eutrophic/hypertrophic scenarios with high biomass of *M. aeruginosa* with variable concentrations of tripton and a_g. Since *M. aeruginosa* is ubiquitous globally, there are many lakes to which these algorithms might apply, for example, Lake Taihu in China (Zhang et al., 2009) and eutrophic lakes in the Netherlands (Dekker, 1993). The approach also demonstrates how species-specific empirical algorithms based on variable $b^*_{b\phi}$ might be derived from red/NIR optical signals.

5 Conclusions

The two-layered sphere model has facilitated in a simplified form the investigation of how a low refractive index particle (a gas vacuole) enclosed within a cell might impact the IOPs of *M. aeruginosa*. The two-layered model was capable of reproducing a number of features attributed to vacuoles: reduction in attenuation and the shift in the chl *a* attenuation peak towards smaller wavelengths with increasing vacuolation; enlarged values for spectral backscattering particularly towards the red and NIR; decreased scattering in the forward direction noticeable as a dip towards smaller angles in the VSF; and an enlargement in the VSF between 30–60°. These findings confirm that gas vacuoles are responsible for these features and that the two-layer model is generally suitable as a first approximation for investigating the influence of gas vacuoles on IOPs in cyanobacteria.

Tuning of the two-layered sphere using Ecolight-S and measured R_{rs} resulted in a mean shell layer $1+\epsilon$ value of 1.12 for a cell with V_g of 50 %. The corresponding values determined for $b^*_{b\phi}(510)$ for *M. aeruginosa* are between 3.8×10^{-3} to $7.2\times10^{-3}\,m^2\,mg^{-1}$. This compares closely to the value measured by Zhou et al. (2012). Simulations using E-S showed how gas vacuolate cells cause the R_{rs} to be greatly

BGD
10, 10531–10579, 2013

enlarged, relative to a population of cells modelled as homogeneous spheres. The changes in R_{rs} can be attributed to variable phytoplankton backscatter caused by intracellular structure (the gas vacuole). Empirical relationships for estimating chl *a* in eutrophic/hypertrophic *M. aeruginosa* blooms derived from the R_{rs} simulations are robust even under variable tripton and gelbstoff concentrations. The empirical algorithms derived here from the bio-optical model might be applicable to other lakes affected by high biomass *M. aeruginosa* blooms. In conclusion, gas vacuoles are one of the most important bio-optical sub-structures profoundly affecting the IOPs of cyanobacteria and leading to increased backscatter in particular towards the red/NIR, which may be distinctive to the genera.

Acknowledgements. The authors gratefully acknowledge the assistance of Lisl Robertson with Ecolight-S. For fieldwork assistance: Trevor Probyn, Heidi van Deventer, Nadine Slabbert. For funding M. W. M.: University of Cape Town and CSIR. The field work was supported by the Department of Water Affairs and the CSIR Safe Waters Earth Observations (SWEOS) research project.

References

Aas, E.: Refractive index of phytoplankton derived from its metabolite composition, J. Plankton Res., 18, 2223–2249, doi:10.1093/plankt/18.12.2223, 1996. 10536, 10539, 10541, 10554

Aden, A. and Kerker, M.: Scattering of electromagnetic waves from two concentric spheres, J. Appl. Phys., 22, 1242–1246, 1951. 10541

Agusti, S. and Phlips, E. J.: Light absorption by cyanobacteria: Implications of the colonial growth form, Limnol. Oceanogr., 37, 434–441, 1992. 10538, 10540, 10553

Ahn, Y. H., Bricaud, A., and Morel, A.: Light backscattering efficiency and related properties of some phytoplankters, Deep-Sea Res., 39, 1835–1855, 1992. 10534, 10539, 10540, 10546, 10549

Arakawa, E. T., Tuminello, P. S., Khare, B. N., and Milham, M. E.: Optical properties of ovalbumin in 0.130-2.50 microm spectral region, Biopolymers, 62, 122–128, doi:10.1002/bip.1004, 2001. 10541

BGD
10, 10531–10579, 2013

Bernard, S., Probyn, T. A., and Barlow, R. G.: Measured and modelled optical properties of particulate matter in the southern Benguela, S. Afr. J. Sci., 97, 410–420, 2001. 10539, 10540, 10543, 10553

Bernard, S., Shillington, F. A., and Probyn, T. A.: The use of equivalent size distributions of natural phytoplankton assemblages for optical modeling, Optics Exp., 15, 1995–2007, 2007. 10540

Bernard, S., Probyn, T. A., and Quirantes, A.: Simulating the optical properties of phytoplankton cells using a two-layered spherical geometry, Biogeosciences Discuss., 6, 1497–1563, doi:10.5194/bgd-6-1497-2009, 2009. 10537, 10541, 10543, 10547

Bidigare, R. R., Schofield, O., and Prezelin, B. B.: Influence of zeaxanthin on quantum yield of photosynthesis of Synechococcus clone WH7803 (DC2)*, Mar. Ecol.-Prog. Ser., 56, 177–188, 1989. 10543

Bricaud, A. and Morel, A.: Light attenuation and scattering by phytoplanktonic cells: a theoretical modeling, Appl. Optics, 25, 571–580, 1986. 10539, 10540, 10544, 10546, 10547, 10548, 10553

Bricaud, A., Morel, A., and Prieur, L.: Optical Efficiency Factors of Some Phytoplankters, Limnol. Oceanogr., 28, 816–832, 1983. 10533

Bricaud, A., Bedhomme, A. L., and Morel, A.: Optical properties of diverse phytoplanktonic species: experimental results and theoretical interpretation, J. Plankton Res., 10, 851–873, 1988. 10547, 10549, 10550

Ciddor, P. E.: Refractive index of air: new equations for the visible and near infrared., Appl. Optics, 35, 1566–1573, 1996. 10541

Dekker, A.: Detection of optical water quality parameters for eutrophic waters by high resolution remote sensing, Ph. D. thesis, Free University, Netherlands, 1993. 10546, 10558

Dekker, A. G., Vos, R. J., and Peters, S. W. M.: Comparison of remote sensing data, model results and in situ data for total suspended matter (TSM) in the southern Frisian lakes, Sci. Total. Environ., 268, 197–214, 2001. 10557

Dekker, A. G., Vos, R. J., and Peters, S. W. M.: Analytical algorithms for lake water TSM estimation for retrospective analyses of TM and SPOT sensor data, Int. J. Remote Sens., 23, 15–35, 2002. 10544

Doxaran, D., Cherukuru, N. C., Lavender, S. J., and Moore, G. F.: Use of a Spectralon panel to measure the downwelling irradiance signal: case studies and recommendations., Appl. Optics, 43, 5981–5986, 2004. 10554

BGD
10, 10531–10579, 2013

Dubelaar, G. B. and van der Reijden, C. S.: Size distributions of Microcystis aeruginosa colonies: a flow cytometric approach, Water Sci. Technol., 32, 171–176, 1995. 10534, 10538
Dubelaar, G. B., Visser, J. W., and Donze, M.: Anomalous behaviour of forward and perpendicular light scattering of a cyanobacterium owing to intracellular gas vacuoles, Cytometry, 8, 405–412, doi:10.1002/cyto.990080410, 1987. 10532, 10533, 10534, 10536, 10540, 10542, 10548, 10549, 10550, 10552
Dupouy, C., Neveux, J., Dirberg, G., Röttgers, R., Barboza Tenório, M. M., and Ouillon, S.: Bio-optical properties of the marine cyanobacteria Trichodesmium spp., J. Appl. Remote Sens., 2, 023503, doi:10.1117/1.2839036, 2008. 10546, 10550
EPA: Methods for chemical analysis of water and wastes, Tech. Rep. 600479020, United States Environmental Protection Agency, Cincinnati, Ohio, 1983. 10544
Fogg, G. E., Stewart, W. D. P., Fay, P., and Walsby, A. E.: Gas vacuoles, in: The Blue-Green Algae, Academic Press, London, 93–110, 1973. 10533
Fuhs, G.: Interferenzmikroskopische beobachtungen an den Polyphosphatkoerpern und gas-vacuolen von cyanophyceen, Osterr. Bot. Z., 116, 411–422, 1969. 10536, 10541, 10547
Ganf, G. G., Oliver, R. L., and Walsby, A. E.: Optical properties of gas-vacuolate cells and colonies of Microcystis in relation to light attenuation in a turbid, stratified reservoir (Mount Bold Reservoir, South Australia), Austr. J. Mar. Freshw. Res., 40, 595–611, 1989. 10532, 10533, 10556
Golecki, J. R. and Drews, G.: Supramolecular organization and composition of membranes, in: The Biology of Cyanobacteria, edited by Carr, N. G. and Whitton, B. A., chap. 6, Blackwell Scientific, Berkeley and Los Angeles, 125–142, 1982. 10542
Hale, G. M. and Querry, M. R.: Optical Constants of Water in the 200-nm to 200-microm Wavelength Region, Appl. Optics, 12, 555–563, 1973. 10541
Johnsen, G., Samset, O., Granskog, L., and Sakshaug, E.: In vivo absorption characteristics in 10 classes of bloom-forming phytoplankton: taxonomic characteristics and responses to photoadaptation by means of discriminant and HPLC analysis, Mar. Ecol.-Prog. Ser., 105, 149–157, 1994. 10543
Jost, M. and Jones, D.: Morphological parameters and macro-molecular organization of gas vacuole membranes of Microcystis aeruginosa Kuetz. emend. Elenkin., Can. J. Microbiol., 16, 159–164, 1970. 10535, 10541
Jost, M. and Zehnder, A.: Die Gasvakuolen der Blaualge Microcystis aeruginosa, Schweiz, Z. Hydrol., 28, 1–3, 1966. 10535

BGD
10, 10531–10579, 2013

Kirk, J. T. O.: A theoretical analysis of the contribution of algal cells to the attenuation of light within natural waters, II. Spherical cells, New Phytol., 75, 21–36, 1975. 10538
Kitchen, J. C. and Zaneveld, J. R. V.: A three-layered sphere model of the optical properties of phytoplankton, Limnol. Oceanogr., 37, 1680–1690, 1992. 10537
Lehmann, H. and Jost, M.: Kinetics of the assembly of gas vacuoles in the blue-green alga Microcystis aeruginosa Kuetz. emend. Elekin., Arch. Microbiol., 79, 59–68, 1971. 10535
Matthews, M. W.: A current review of empirical procedures of remote sensing in inland and near-coastal transitional waters, Int. J. Remote Sens., 32, 6855–6899, doi:10.1080/01431161.2010.512947, 2011. 10557
Matthews, M. W., Bernard, S., and Winter, K.: Remote sensing of cyanobacteria-dominant algal blooms and water quality parameters in Zeekoevlei, a small hypertrophic lake, using MERIS, Remote Sens. Environ., 114, 2070–2087, 2010. 10556
Matthews, M. W., Bernard, S., and Robertson, L.: An algorithm for detecting trophic status (chlorophyll-a), cyanobacterial-dominance, surface scums and floating vegetation in inland and coastal waters, Remote Sens. Environ., 124, 637–652, doi:10.1016/j.rse.2012.05.032, 2012. 10534, 10556, 10557
Meffert, M. E., Oberhäuser, R., and Overbeck, J.: Morphology and taxonomy of Oscillatoria redekei (Cyanophyta), Br. Phycol. J., 16, 107–114, 1981. 10535
Mitchell, B. G., Kahru, M., Wieland, J., and Stramska, M.: Determination of spectral absorption coefficients of particles, dissolved material and phytoplankton for discrete water samples, in: Ocean Optics Protocols For Satellite Ocean Color Sensor Validation, Revision 4, Volume IV: Inherent Optical Properties: Instruments, Characterizations, Field Measurements and Data Analysis Protocols, edited by: Mueller, J. L., Fargion, G. S., and McClain, C. R., chap. 4, National Aeronautical and Space Administration, Greenbelt, Maryland, 125–153, 2003. 10539
Morel, A. and Bricaud, A.: Inherent optical properties of algal cells including picoplankton: Theoretical and experimental results, Can. Bull. Fish. Aquat. Sci, 214, 521–559, 1986. 10538, 10540, 10542, 10547, 10550
Morel, A., Ahn, Y.-H., Partensky, F., Vaulot, D., and Claustre, H.: Prochlorococcus and Synechococcus: A comparative study of their optical properties in relation to their size and pigmentation, J. Mar. Res., 51, 617–649, doi:10.1357/0022240933223963, 1993. 10538
Mueller, J. L., Morel, A., Frouin, R., Davis, C., Arnone, R., Carder, K., Lee, Z., Steward, R., Hooker, S., Mobley, C. D., McLean, S., Holben, B., Miller, M., Pietras, C., Knobelspiesse, K. D., Fargion, G. S., Porter, J., and Voss, K.: Radiometric measurements and data

BGD
10, 10531–10579, 2013

analysis protocols, in: Ocean Optics Protocols For Satellite Ocean Color Sensor Validation, Revision 4, Volume III:, edited by: James, L., Mueller, G. S. F., and McClain, C. R., vol. III, NASA, Goddard Space Flight Space Center, Greenbelt, Maryland, 78 pp., 2003. 10545

Ogawa, T., Sekine, T., and Aiba, S.: Reappraisal of the so-called light shielding of gas vacuoles in Microcystis Aeruginosa, Arch. Microbiol., 122, 57–60, 1979. 10533, 10535, 10549

Petzold, T. J.: Volume scattering functions for selected ocean waters, Tech. rep., Scripps Institution of Oceanography Visibility Laboratory, San Diego, California, available at: http://oai.dtic.mil/oai/oai?verb=getRecord&metadataPrefix=html&identifier=AD0753474, 1972. 10551, 10574

Porter, J. and Jost, M.: Physiological effects of the presence and absence of gas vacuoles in the blue-green alga, Microcystis aeruginosa Kuetz. emend. Elenkin, Arch. Microbiol., 110, 225–231, 1976. 10536, 10542

Quinby-Hunt, M., Hunt, A., Lofftus, K., and Shapiro, D.: Polarized-light scattering studies of marine chlorella, Limnol. Oceanogr., 34, 1587–1600, 1989. 10537, 10542, 10547, 10551, 10554

Quirantes, A. and Bernard, S.: Light-scattering methods for modelling algal particles as a collection of coated and/or nonspherical scatterers, J. Quant. Spectrosc. Radiat. T., 100, 315–324, 2006. 10537

Rajagopal, S., Sicora, C., Várkonyi, Z., Mustárdy, L., and Mohanty, P.: Protective effect of supplemental low intensity white light on ultraviolet-B exposure-induced impairment in cyanobacterium Spirulina platensis: formation of air vacuoles as a possible protective measure., Photosynth. Res., 85, 181–189, doi:10.1007/s11120-005-2439-6, 2005. 10535

Randolph, K., Wilson, J., Tedesco, L., Li, L., Pascual, D. L., and Soyeux, E.: Hyperspectral remote sensing of cyanobacteria in turbid productive water using optically active pigments, chlorophyll a and phycocyanin, Remote Sens. Environ., 112, 4009–4019, 2008. 10556

Raven, J. A.: The Role of Vacuoles, New Phytol., 106, 357–422, 1987. 10536

Retalis, A., Hadjimitsis, D. G., Michaelides, S., Tymvios, F., Chrysoulakis, N., Clayton, C. R. I., and Themistocleous, K.: Comparison of aerosol optical thickness with in situ visibility data over Cyprus, Nat. Hazards Earth Syst. Sci., 10, 421–428, doi:10.5194/nhess-10-421-2010, 2010. 10545

Reynolds, C. S.: The Ecology of Phytoplankton, Cambridge University Press, New York, 2006. 10544

BGD
10, 10531–10579, 2013

Reynolds, C. S., Jaworski, G. H. M., Cmiech, H. A., and Leedale, G. F.: On the annual cycle of the blue-green alga microcystis aeruginosa kutz. Emend. Elenkin, Philos. T. R. Soc. London B, 293, 419–477, 1981. 10536, 10537, 10538, 10540, 10553

Robarts, A. R. D., Zohary, T., and Robarts, R. D.: Microcystis aeruginosa and underwater light attenuation in a hypertrophic lake (Hartbeespoort Dam, South Africa), J. Ecol., 72, 1001–1017, 1984. 10540

Roesler, C.: Theoretical and experimental approaches to improve the accuracy of particulate absorption coefficients derived from the quantitative filter technique, Limnol. Oceanogr., 43, 1649–1660, 1998. 10540

Rottgers, R., Doerffer, R., McKee, D., and Schonfeld, W.: Algorithm Theoretical Basis Document: The Water Optical Properties Processor (WOPP), Tech. rep., Helmholtz-Zentrum Geesthacht, University of Strathclyde, Geesthacht, 1–20, 2011. 10545

Sartory, D. P. and Grobbelaar, J. U.: Extraction of chlorophyll a from freshwater phytoplankton for spectrophotometric analysis, Hydrobiologia, 114, 177–187, 1984. 10539

Schreurs, R.: Light scattering by algae: fitting experimental data using Lorenz-Mie theory, Ph. D. thesis, Vrije University, Amsterdam, 1996. 10534, 10550, 10551

Shear, H. and Walsby, A. E.: An investigation into the possible light-shielding role of gas vacuoles in a planktonic blue-green alga, European J. Phycol., 10, 241–251, doi:10.1080/00071617500650231, 1975. 10533, 10534, 10535, 10536, 10537

Smith, R. V. and Peat, A.: Comparative structure of the gas-vacuoles of blue-green algae, Arch. Microbiol., 57, 111–122, 1967. 10542

Spinrad, R. W. and Brown, J. F.: Relative real refractive index of marine microorganisms: a technique for flow cytometric estimation, Appl. Optics, 12, 25, 1930–1934, 1986. 10547

Stramski, D. and Wozniak, S. B.: On the role of colloidal particles in light scattering in the ocean, Limnol. Oceanogr., 50, 1581–1591, 2005. 10544

Stramski, D., Bricaud, A., and Morel, A.: Modeling the inherent optical properties of the ocean based on the detailed composition of the planktonic community, Appl. Optics, 40, 2929–2945, 2001. 10536, 10538, 10544

Svensen, O., Frette, O., and Erga, S. R.: Scattering properties of microalgae: the effect of cell size and cell wall, Appl. Optics, 46, 5762–5769, 2007. 10532, 10542, 10551, 10554

Toon, O. B. and Ackerman, T. P.: Algorithms for the calculation of scattering by stratified spheres, Appl. Optics, 20, 3657–3660, 1981. 10541

BGD
10, 10531–10579, 2013

Vaillancourt, R. D.: Light backscattering properties of marine phytoplankton: relationships to cell size, chemical composition and taxonomy, J. Plankton Res., 26, 191–212, doi:10.1093/plankt/fbh012, 2004. 10555

Van Baalen, C. and Brown, R. M.: The ultrastructure of the marine blue green alga, Trichodesmium erythraeum, with special reference to the cell wall, gas vacuoles, and cylindrical bodies, Arch. Microbiol., 69, 79–91, 1969. 10535

van Liere, L. and Walsby, A. E.: Interactions of cyanobacteria with light, in: The Biology of Cyanobacteria, edited by: Carr, N. G. and Whitton, B. A., chap. 2, Blackwell Scientific, Berkeley and Los Angeles, 9–46, 1982. 10533

Volten, A. H., Haan, J. F. D., Hovenier, J. W., Schreurs, R., Vassen, W., Dekker, A. G., Hoogenboom, J., Charlton, F., and Wouts, R.: Laboratory Measurements of Angular Distributions of Light Scattered by Phytoplankton and Silt, Limnol. Oceanogr., 43, 1180–1197, 1998. 10532, 10534, 10547, 10550, 10551, 10552, 10574, 10575

Šmarda, J.: Cell ultrastructure changes accompanying the annual life cycle of the cyanobacterium Microcystis aeruginosa, Algolog. Stud., 130, 27–38, doi:10.1127/1864-1318/2009/0130-0027, 2009. 10535, 10536, 10537, 10542

Waaland, J. R., Waaland, S. D., and Branton, D.: Gas vacuoles: Light shielding in blue-green algae, J. Cell Biol., 48, 212–215, 1971. 10533, 10535

Walsby, A. E.: Gas vesicles, Microbiological reviews, 58, 94–144, doi:10.1016/j.tim.2006.01.002, 1994. 10533, 10535, 10541

Wang, Q., Sun, D., Li, Y., Le, C., and Huang, C.: Mechanisms of remote-sensing reflectance variability and its relation to bio-optical processes in a highly turbid eutrophic lake: Lake Taihu (China), IEEE T. Geosci. Remote, 48, 575–584, doi:10.1109/TGRS.2009.2027316, 2010. 10556

Whitmire, A. L., Pegau, W. S., Karp-boss, L., Boss, E., and Cowles, T. J.: Spectral backscattering properties of marine phytoplankton cultures, Optics Exp., 18, 1680–1690, doi:10.1364/OE.18.015073, 2010. 10532, 10534, 10536, 10550, 10555

Witkowski, K., Krol, T., Zielinski, A., and Kuten, E.: A light-scattering matrix for unicellular marine phytoplankton, Limnol. Oceanogr., 43, 859–869, 1998. 10551

Zhang, X., Lewis, M., Lee, M., Johnson, B., and Korotaev, G.: The volume scattering function of natural bubble populations, Limnol. Oceanogr., 47, 1273–1282, doi:10.4319/lo.2002.47.5.1273, 2002. 10551

BGD
10, 10531–10579, 2013

Zhang, Y., Liu, M., Qin, B., van der Woerd, H. J., Li, J., and Y, L.: Modeling remote-sensing reflectance and retrieving chlorophyll-a concentration in extremely turbid case-2 waters (Lake Taihu, China), IEEE T. Geosci. Remote, 47, 1937–1948, 2009. 10544, 10558

Zhang, Y., Yin, Y., Wang, M., and Liu, X.: Effect of phytoplankton community composition and cell size on absorption properties in eutrophic shallow lakes: field and experimental evidence, Optics Exp., 20, 11882–11898, doi:10.1364/OE.20.011882, 2012. 10546

Zhou, W., Wang, G., Sun, Z., Cao, W., Xu, Z., Hu, S., and Zhao, J.: Variations in the optical scattering properties of phytoplankton cultures, Optics Exp., 20, 11189–11206, 2012. 10533, 10534, 10536, 10540, 10547, 10549, 10550, 10552, 10553, 10554, 10555, 10558, 10569, 10576

Zimba, P. V. and Gitelson, A.: Remote estimation of chlorophyll concentration in hyper-eutrophic aquatic systems: model tuning and accuracy optimization, Aquaculture, 256, 272–286, 2006. 10556

BGD
10, 10531–10579, 2013

Table 1. Chl *a* specific volume coefficients ($m^2\,mg^{-1}$), efficiency factors and scattering probabilities (%) at 510 nm for a population of *M. aeruginosa* modelled as two-layered spheres with variable gas vacuole content (%) for shell layers $1+\epsilon = 1.080$ and $1+\epsilon = 1.036$.

V_g	c^*_ϕ	b^*_ϕ	$b^*_{b\phi}\times10^3$	Q_c	Q_b	Q_{bb}	$\tilde{b}_{b\phi}$	$\tilde{b}_{f\phi}$
$1+\epsilon=1.080$								
0	0.27	0.25	1.0	2.00	1.85	0.0073	0.39	99.59
3	0.28	0.26	1.2	2.09	1.94	0.0087	0.45	99.54
10	0.32	0.30	1.4	2.34	2.18	0.0106	0.49	99.50
30	0.35	0.33	1.8	2.60	2.44	0.0134	0.55	99.44
50	0.35	0.33	2.1	2.60	2.45	0.0156	0.64	99.35
$1+\epsilon=1.036$								
0	0.38	0.36	0.1	2.77	2.62	0.0004	0.02	99.96
3	0.35	0.33	0.2	2.59	2.44	0.0015	0.06	99.92
10	0.33	0.31	0.4	2.42	2.28	0.0029	0.13	99.85
30	0.25	0.23	0.8	1.84	1.70	0.0055	0.32	99.66
50	0.24	0.22	1.0	1.73	1.59	0.0077	0.48	99.51

BGD
10, 10531–10579, 2013

Table 2. Effect of variable c_i on the complex refractive index and IOPs (510 nm) of a population of vacuolate cells (V_g = 50 %).

c_i (kg m^{-3})	2.096	3.16	4.525
$\overline{Q_a}(675)$	0.145	0.219	0.313
$n'(675)$	0.0017	0.0026	0.0041
$1+\epsilon$	1.0801	1.0801	1.0805
Q_b	2.45	2.36	2.27
Q_{bb}	0.016	0.015	0.014
b^*_ϕ (m^2 mg^{-1})	0.33	0.21	0.14
$b^*_{b\phi}$ (m^2 mg^{-1})	0.0021	0.0013	0.0008
$\widetilde{b}_{b\phi}$ (m^2 mg^{-1})	0.0064	0.0062	0.0060

BGD
10, 10531–10579, 2013

Table 3. Optical efficiency factors and chl *a* specific volume coefficients ($m^2\,mg^{-1}$) at 510 nm for a population of *M. aeruginosa* modelled as a population of two-layered spheres with $1+\epsilon = 1.12$ and $V_g = 50\,\%$.

	Q_c	Q_b	Q_{bb}	c^*_ϕ	b^*_ϕ	$b^*_{b\phi} \times 10^3$	$\tilde{b}_{bb}$ (%)
Two layered spheres	2.35	2.20	0.040	0.321	0.30	5.5	1.8
Zhou et al. (2012)	–	2.26	0.020	–	0.6326	5.7	0.91

BGD
10, 10531–10579, 2013

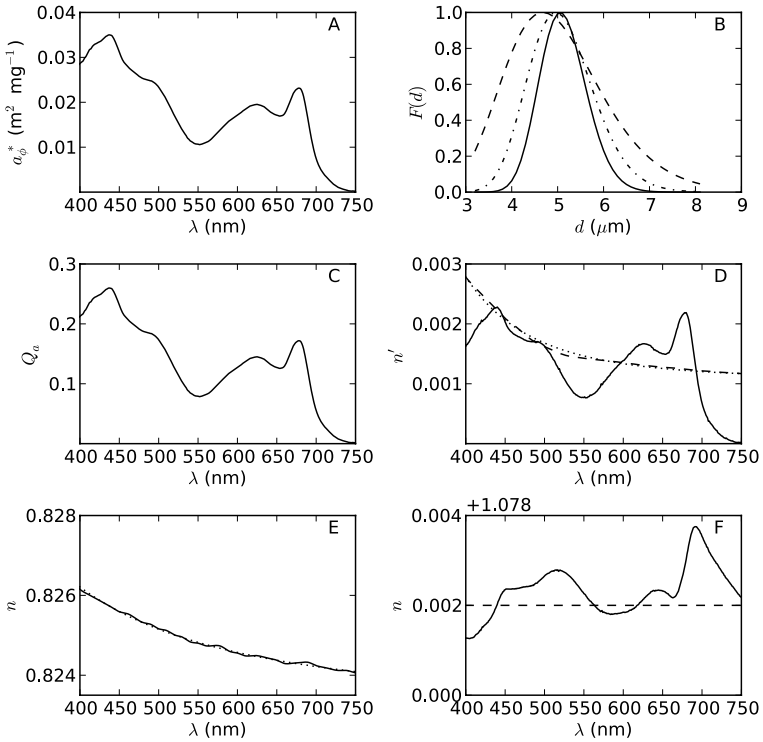

Fig. 1. Optical and size parameters for *M. aeruginosa* and gas vacuole. **(A)** chl *a* specific absorption, **(B)** normalised log-normal PSD for $V_{\text{eff}} = 0.01$ (–), $V_{\text{eff}} = 0.02$ (- ·), and $V_{\text{eff}} = 0.05$ (- -), **(C)** Experimental absorption efficiency factor, **(D)** imaginary refractive indices for *M. aeruginosa* (–) and gas vacuole (- -) $\times 1e^2$, showing best fit line (··) **(E)** real refractive index for gas vacuole showing best fit line (··), **(F)** real refractive index for *M. aeruginosa* (–) showing $1 + \epsilon$ value (- -).

BGD
10, 10531–10579, 2013

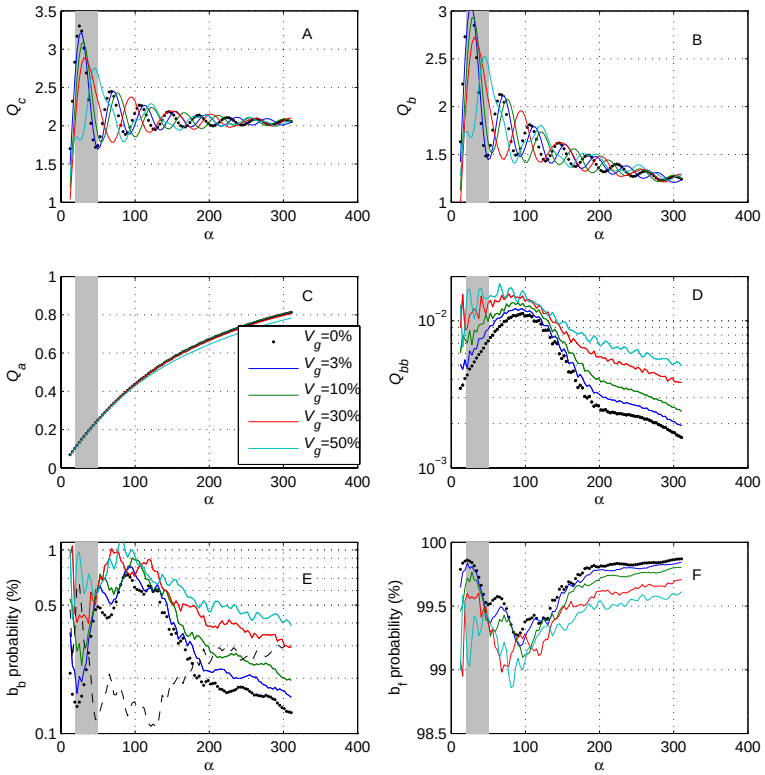

Fig. 2. Optical efficiency factors and the backward and forward scattering probabilities of *M. aeruginosa* versus the Mie size parameter, α, modelled as two-layered spheres with variable gas vacuolation (0–50 % cell volume). Plotted for cell diameters from 1–50 µm at λ = 675 nm. The shading indicates the size range applicable to *M. aeruginosa*. The dotted line in **E** is the ratio of backscattering probability where V_g = 50 % to that where V_g = 0 % × 10^{-1}.

BGD
10, 10531–10579, 2013

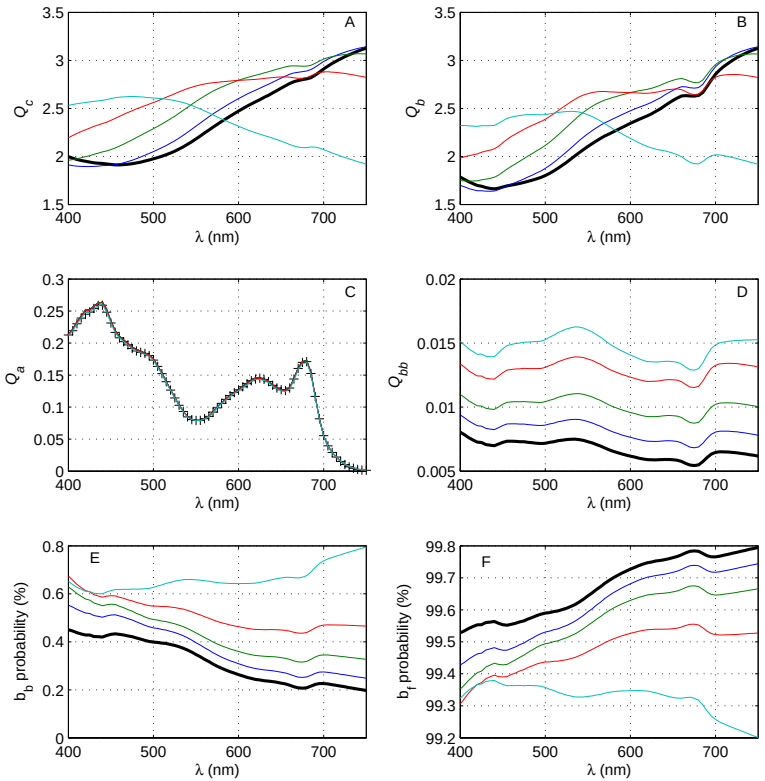

Fig. 3. Optical efficiency factors and forward and backward scattering probabilities of a population of *M. aeruginosa* modelled as two-layered spheres with variable gas vacuolation (0–50 % cell volume). Legend is the same as Fig. 2. The measured absorption efficiency factor is drawn for comparison in C (+).

BGD
10, 10531–10579, 2013

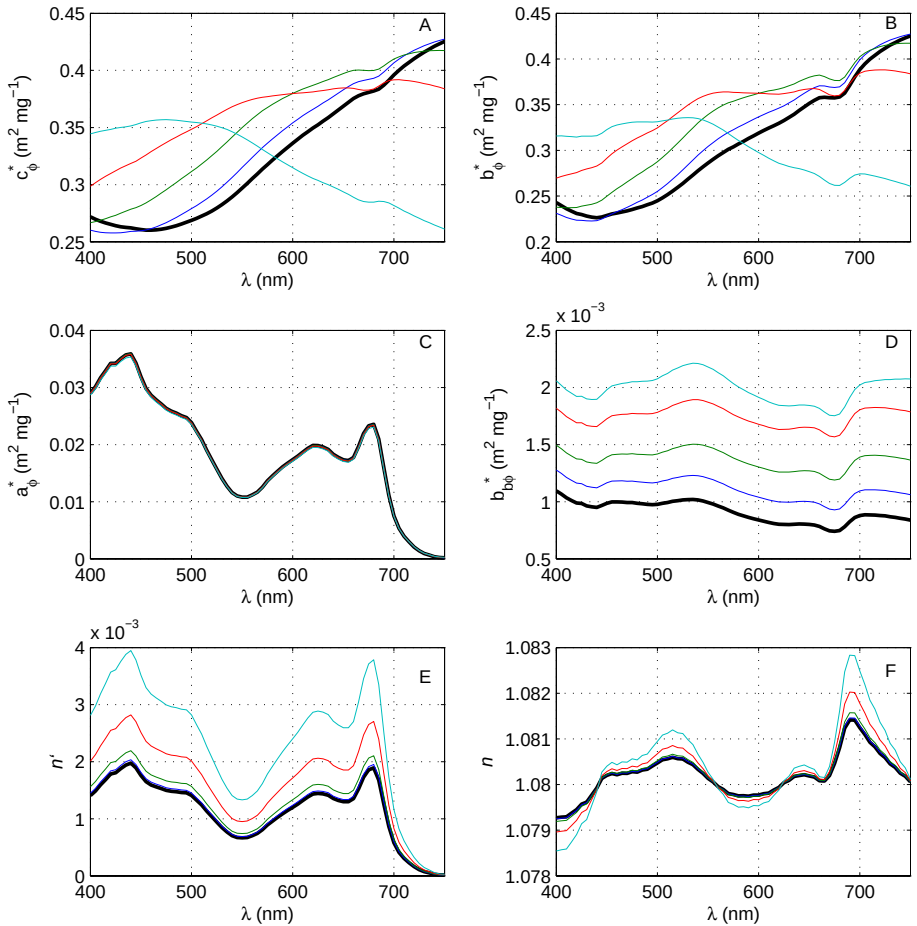

Fig. 4. Chl *a* specific volume coefficients for a population of *M. aeruginosa* modelled as two-layered spheres with variable gas vacuolation (**A**–**D**). Legend same as Fig. 2. The influence of gas vacuolation on the imaginary and real refractive index are also shown (**E** and **F**).

BGD
10, 10531–10579, 2013

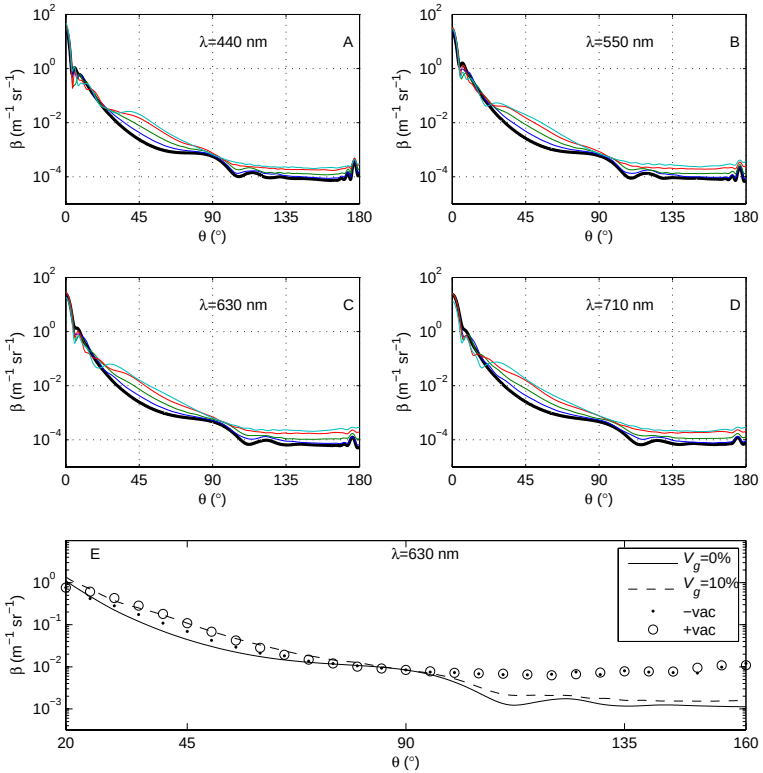

Fig. 5. Volume scattering functions for a population of *M. aeruginosa* at various wavelengths modelled as two-layered spheres with variable gas vacuolation (0–50 % cell volume). Legend same as Fig. 2. **(E)** shows comparison of these results with measurements of vacuolate (+vac) and non-vacuolate (−vac) *M. aeruginosa* made by Volten et al. (1998) at 633 nm (scaled to San Diego Harbor measurements of Petzold, 1972, at 90˚).

BGD
10, 10531–10579, 2013

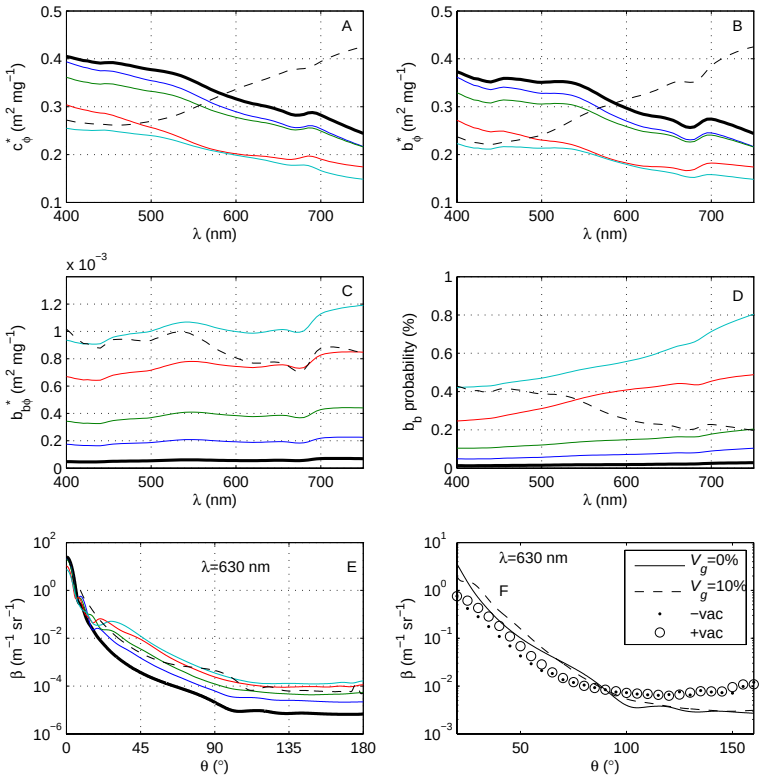

Fig. 6. Chl *a* specific IOPs and VSFs for a population of *M. aeruginosa* modelled as two-layered spheres with variable gas vacuolation (0–50 % cell volume) and $1 + \epsilon = 1.036$. The dotted line in **(A)**–**(E)** is for a cell with $V_g = 0\,\%$ and $1 + \epsilon = 1.080$. Legend same as Fig. 2. **(F)** shows comparison with measurements of Volten et al. (1998) (see Fig. 5 for details).

BGD
10, 10531–10579, 2013

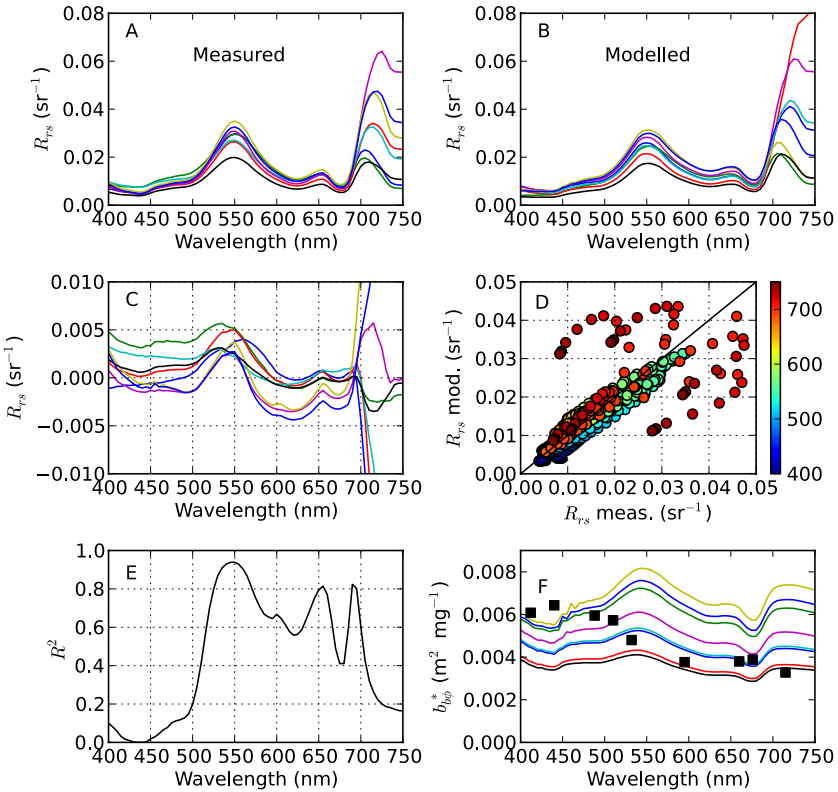

Fig. 7. Tuning of the two-layered sphere model using measured R_{rs}. **(A)** Measured and **(B)** modelled R_{rs}. **(C)** The difference between the measured and modelled R_{rs}. **(D)** Scatterplot of measured and modelled reflectance colored by wavelength. **(E)** Wavelength-specific R^2 between measured and modelled R_{rs} ($N = 8$). **(F)** $b^*_{b\phi}$ corresponding to various shell layer $1 + \epsilon$ values determined by fitting the measured and modelled R_{rs}, and that measured by Zhou et al. (2012) (squares).

BGD
10, 10531–10579, 2013

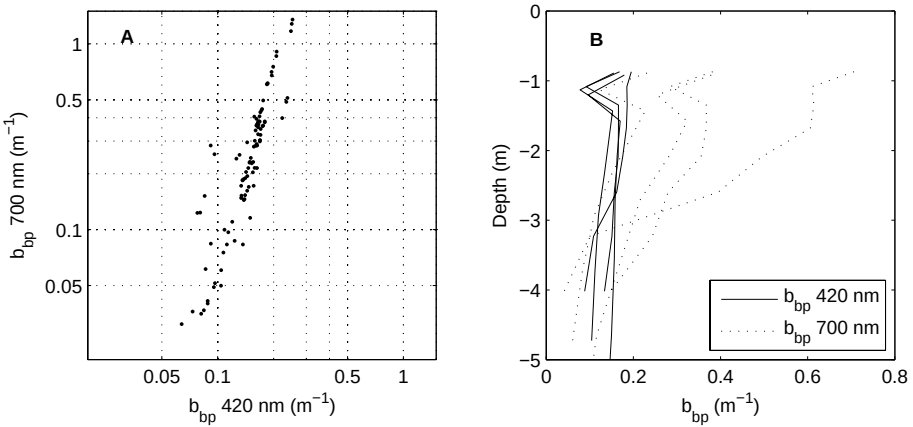

Fig. 8. (A) $b_{bp}(700)$ versus $b_{bp}(420)$ from 11 profiles. Note exponential relationship with log-scaled axes. **(B)** Five selected depth profiles with minimum depth of 0.8 m. Note that $b_{bp}(420) > b_{bp}(700)$ at depth.

BGD
10, 10531–10579, 2013

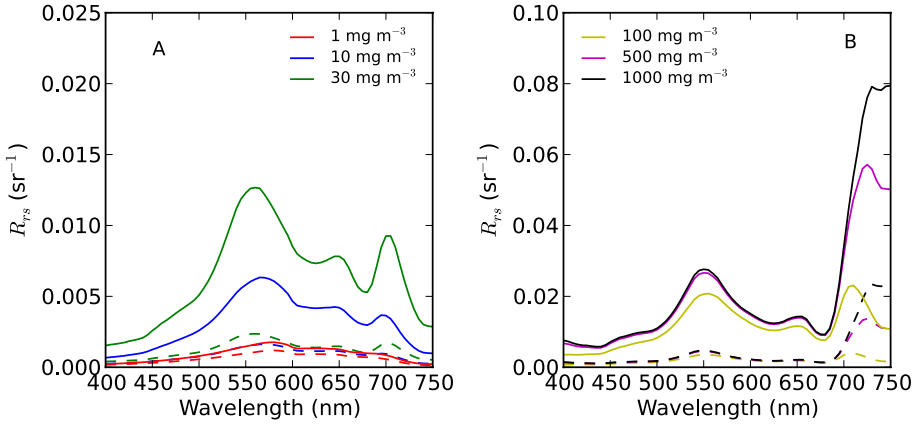

Fig. 9. R_{rs} modelled at various concentrations of chl *a* showing difference between vacuolate (solid lines) and non-vacuolate (dotted lines) populations of *M. aeruginosa*. Vacuolate cells were modelled with shell $1+\epsilon$ of 1.12 and $V_g = 50\,\%$. Non-vacuolate cells were homogeneous cells with $1+\epsilon$ of 1.080. The values for $a_{tr}(440)$ and $a_g(440)$ were constant at $0.5\,m^{-1}$ and $1.5\,m^{-1}$, respectively. For more details see text.

BGD
10, 10531–10579, 2013

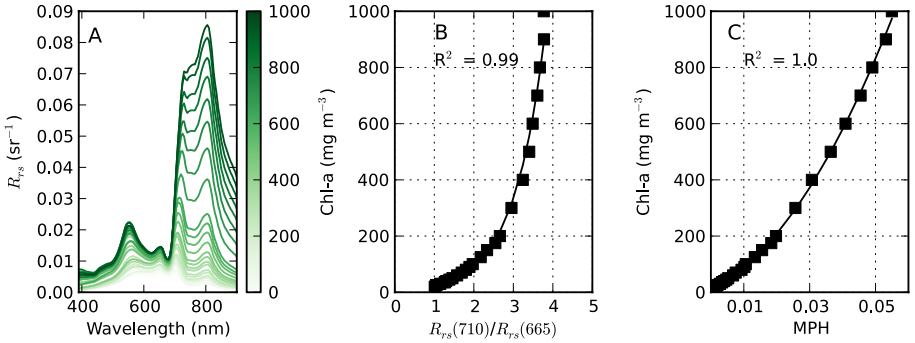

Fig. 10. (A) R_{rs} simulated for chl *a* between 20 and 1000 mg m^{-3} for a vacuolate *M. aeruginosa* population with random perturbations in tripton concentration and $a_g(440)$. Empirical relationships between chl *a* and **(B)** the 710 : 665 band ratio and **(C)** the MPH variable showing the best fit lines.

BGD
10, 10531–10579, 2013